Biomaterials 252 (2020) 120104

Contents lists available at ScienceDirect

Biomaterials

journal homepage: www.elsevier.com/locate/biomaterials

Engineered 3D hydrogels with full-length fibronectin that sequester and present growth factors

Sara Trujillo[a], Cristina Gonzalez-Garcia[a], Patricia Rico[b], Andrew Reid[c], James Windmill[c], Matthew J. Dalby[a], Manuel Salmeron-Sanchez[a,*]

[a] Centre for the Cellular Microenvironment, University of Glasgow, Glasgow, United Kingdom
[b] Biomedical Research Networking Centre in Bioengineering Biomaterials and Nanomedicine, Universitat Politècnica de València, Valencia, Spain
[c] Centre for Ultrasonic Engineering, Department of Electronic and Electrical Engineering, University of Strathclyde, Glasgow, United Kingdom

ARTICLE INFO

Keywords:
Hydrogels
Growth factors
Fibronectin
poly(ethylene) glycol
Bone
Vascularisation

ABSTRACT

Extracellular matrix (ECM)-derived matrices such as Matrigel are used to culture numerous cell types in vitro as they recapitulate ECM properties that support cell growth, organisation, migration and differentiation. These ECM-derived matrices contain various growth factors which make them highly bioactive. However, they suffer lot-to-lot variability, undefined composition and lack of controlled physical properties. There is a need to develop rationally designed biomaterials that can also recapitulate ECM roles. Here, we report the development of fibronectin (FN)-based 3D hydrogels of controlled stiffness and degradability that incorporate full-length FN to enable solid-phase presentation of growth factors in a physiological manner. We demonstrate, in vitro and in vivo, the effect of incorporating vascular endothelial growth factor (VEGF) and bone morphogenetic protein 2 (BMP2) in these hydrogels to enhance angiogenesis and bone regeneration, respectively. These hydrogels represent a step-change in the design of well-defined, reproducible, synthetic microenvironments for 3D cell culture that incorporate growth factors to achieve functional effects.

1. Introduction

In 3D culture, ECM-derived matrices, such as Matrigel, are currently widely used and support the growth and function of a wide variety of cell types in vitro, including the formation of organoids, cancer studies and cell engineering [1–4]. However, Matrigel is an undefined mixture of ECM proteins and growth factors (GFs) obtained from Engelbreth-Holm-Swarm mouse sarcoma cells [5]. Matrigel composition is undefined, lacking control of mechanical properties and subjected to lot-to-lot variability. Given this, there is a pressing need to design biomaterials that can fulfil the roles of the ECM. However, biomaterials that have similar stiffness of the target tissue, degradability and that can present adhesion motifs and GFs with enhanced potency compared to soluble GFs, have yet to be identified. It is for this reason that Matrigel is widely used – as it contains proteins and GFs that provide biological activity not yet achieved by synthetic systems.

GFs are signalling molecules that play essential roles in tissue development and organogenesis. GFs drive cell differentiation and stimulate cell migration and proliferation [6]. Given these roles, GFs have potential clinical utility, particularly in regenerative medicine [7,8]. Despite this, the potential of GFs has yet to be fully realised in medicine, partly due to their short half-life and rapid clearance in vivo [9,10]. The ECM acts as a reservoir that binds GFs and coordinates their availability for cell interactions [11]. For example, the glycosaminoglycan heparin, has been incorporated into hydrogels to sequester GFs for tissue-engineering applications [12]. Other proteins, such as fibrinogen, tenascin C or fibronectin (FN) are also known to bind GFs [13–15]. In particular, FN is an ECM protein widely used to study cell response, e.g. in mechanotransduction studies. Classically, FN has been adsorbed onto a wide range of surfaces [16,17] including synthetic hydrogels such as polyacrylamide (PAAm) [18] or poly(ethylene) glycol (PEG) [19]. Depending on the properties of the surface, adsorption leads to different conformations, promoting better adhesion properties on hydrophilic surfaces [20], promoting unfolding [21], fibrillogenesis [22] or different binding to several integrins [23]. FN promiscuously binds GFs, including therapeutically relevant GFs, such as bone morphogenetic protein 2 (BMP2, which drives bone formation) [24] and vascular endothelial GF (VEGF, which stimulates angiogenesis) [15]. Importantly, FN presents the GF-binding site ($FNIII_{12\text{-}14}$) next to the integrin-binding site ($FNIII_{9\text{-}10}$). This can trigger the simultaneous binding of integrins

* Corresponding author. Centre for the Cellular Microenvironment, James Watt School of Engineering, Rankine Building, University of Glasgow, 79-85 Oakfield Avenue, Glasgow, G12 8LT, UK.
E-mail address: Manuel.Salmeron-Sanchez@glasgow.ac.uk (M. Salmeron-Sanchez).

https://doi.org/10.1016/j.biomaterials.2020.120104
Received 8 November 2019; Received in revised form 4 May 2020; Accepted 5 May 2020
Available online 07 May 2020

and GF receptors leading to synergistic integrin/GF receptor signalling, which enhances the effect of GFs on stem cell differentiation and tissue repair and regeneration [13,25–28].

Material-based strategies have been developed to control GF sequestration and release, in order to reduce their dosage and to control their local action [11,29–33] including materials that exploit this synergistic integrin/GF interaction [34]. Such approaches include the use of cell-mediated FN fibrillogenesis [35,36], which lacks substantial 3D structure, or the use of materials that promote FN assembly [37]. On the latter for example, poly(ethyl acrylate) (PEA) is a polymer that causes FN to spontaneously unfold and assemble into nanonetworks, exposing the $FNIII_{9\text{-}10}$ and $FNIII_{12\text{-}14}$ binding sites to cells to enable the delivery of ultra-low doses of GFs [37–39]. FN assembled on PEA has been used to successfully present BMP2 in a murine non-healing (critical-size) bone defect model [40] and in a veterinary case of a dog with a non-union humeral fracture [39]. This PEA polymer can be used as a coating for other scaffold materials to target the efficient presentation of GFs by altering FN's conformation [39].

In 3D, fibrin hydrogels have been functionalised with FN fragments that contain both the cell adhesion site ($FNIII_{9\text{-}10}$) and the GF binding site ($FNIII_{12\text{-}14}$) [25]. These hydrogels, loaded with VEGF, promote wound healing in diabetic mice and, loaded with BMP2, bone regeneration in a rat non-healing bone defect model [25]. Fibrin hydrogels are formed by fibrinogen clotting and so fibrinogen has been incorporated in PEG hydrogels to deliver BMP2 [41]. Critically, FN, like fibrinogen, is an abundant soluble protein in plasma. However, FN is also present in the insoluble part of the ECM. In this context, the ability of FN to bind GFs helps the ECM to regulate their bioavailability during both homeostasis and tissue repair. Full-length FN presents many other binding sites apart from the cell adhesion domain and the growth factor binding sites, which are physiologically relevant. For instance, FN contains two binding sites ($FNI_{1\text{-}5}$ and $FNIII_{12\text{-}14}$) for proteoglycans, such as syndecan-2 and -4, that trigger focal adhesion assembly via protein kinase C alpha (PKCα) and focal adhesion kinase (FAK) [42,43]. Also, the variable region of FN contains the Leu-Asp-Val (LDV) and the Arg-Glu-Asp-Val (REDV) sequences that bind $\alpha_4\beta_1$ and $\alpha_4\beta_7$ integrins (non RGD-binding integrins) [44,45]. FN also contains FN-binding sites that are essential for FN fibrillogenesis ($FNI_{1\text{-}5}$, $FNIII_{1\text{-}2}$, $FNIII_7$, $FNIII_{10}$ and $FNIII_{12\text{-}15}$), and contribute to vascular morphogenesis [46,47]. FN also has binding sites for collagen and fibrin, among other molecules, demonstrating the versatile role of FN within the ECM [48–50]. Therefore, the use of full-length FN in synthetic hydrogels is expected to be advantageous as it recapitulates better than FN fragments the rich biological activity of FN within the ECM.

The ability to mimic the role of the ECM in GF presentation is key to developing effective materials-based approaches for 3D culture and regenerative medicine. The physiological, solid-state presentation of GFs is also required as their soluble delivery has significant limitations. For example, clinically, soluble delivery of supraphysiological doses is required due to the short half-life of unbound GFs and to their clearance from the site. BMP2 represents an instructive example of the issues that can arise with traditional GF administration. The use of recombinant human (rh)BMP2 was approved by the Food and Drug Administration (FDA) in 2002 and has since then revolutionised the bone graft substitute market [51,52]. The concentration of BMP2 approved by the FDA for human use is 1.5 mg mL^{-1}. This high dose has led to increased incidence of adverse effects, including inflammation, ectopic bone and tumour formation, wound and urogenital complications [53].

To provide an alternative to natural ECM-derived matrices and to overcome some of the limitations of synthetic ones such as poor cell attachment, lack of cell-mediated degradability or absence of solid phase presentation of GFs [54,55], we report here the development of synthetic 3D hydrogels that incorporate full-length FN. As a proof of concept, we demonstrate two examples of important applications in cell and tissue engineering: vascularisation studies in vitro and bone regeneration in vivo. Bone is the second most-transplanted tissue after blood [56]. With bone autografts in short supply and with allografts being poorly bioactive [57,58], there is still a need for materials that can improve bone growth [59,60]. Angiogenesis is also of paramount importance to the health and survival of new or regenerating tissue [61]. In fact, both angiogenesis and osteogenesis are vital processes in acute fracture healing and bone repair [62]. Our hydrogels contain full length, human FN, enabling ultra-low dose, solid-phase presentation of GFs. In particular, we functionalise the FN protein with PEG-maleimide (i.e. PEGylation of full-length FN) in order to covalently crosslink the protein to the synthetic hydrogel network. In this case, the hybrid polymer-FN network consists of 4-arm-PEG-maleimide crosslinked with PEG-dithiol and thiolated, protease-degradable peptides. We demonstrate that the physical properties of this hydrogel can be tuned to recapitulate the properties of native ECM. Using BMP2 and VEGF, we demonstrate the ability of this hydrogel system to recruit and retain GFs in vitro, thereby providing a novel 3D, functional environment with the potential to replace Matrigel, and to promote bone regeneration and vascularisation in vivo.

2. Materials and methods

2.1. Fibronectin PEGylation

Fibronectin (FN, YoProteins, 3 mg mL^{-1}) was PEGylated by modifying a previously published procedure [63]. FN was denatured in denaturing buffer (denaturing buffer: 5 mM Tris(2-carboxyethyl)phosphine hydrochloride (TCEP, pH 7, Sigma) and 8 M urea (Acros Organics, 99.5%) in phosphate buffer saline (PBS, Gibco, pH 7.4)) for 15 min at room temperature (RT). Then, 4-arm-PEG-Maleimide (PEGMAL, 20 kDa, LaysanBio) was incubated for 30 min at RT at a molar ratio FN:PEGMAL 1:4. After PEGylation, remaining non-reacted cysteine residues were blocked by alkylation using 14 mM iodoacetamide (Sigma) in PBS at pH 8 for 2 h. The product of the reaction was dialysed using (Mini-A-Lyzer, MWCO 10 KDa, ThermoFisher) against PBS for 1 h at RT. The protein solution was then precipitated using cold ethanol. Briefly, nine volumes of cold absolute ethanol were added to the protein solution and mixed using a vortex mixer. The mixture was then incubated at −20 °C overnight and centrifuged at 15,000 g and 4 °C for 15 min. The supernatant was discarded, and the protein pellet was further washed with 90% cold ethanol and centrifuged again at 15,000 g and 4 °C for 5 min. Pellets were dried and solubilised using 8 M urea at a final protein concentration of 2.5 mg mL^{-1}. Once the protein was dissolved, the solution was dialysed against PBS for 1 h and stored in the freezer or immediately used.

2.2. Hydrogel formation

PEG hydrogels were formed using Michael-type addition reaction under physiological pH and temperature following a previously published protocol [31]. Briefly, a final concentration of 1 mg mL^{-1} of PEGylated FN was added to different amounts of PEGMAL (3 wt%, 5 wt % or 10 wt%). The thiolated crosslinker was added always at the end, at a molar ratio 1:1 maleimide:thiol to ensure full crosslinking. The crosslinkers used were either PEG-dithiol (PEGSH, 2 kDa, Creative PEGWorks) or mixtures of PEGSH and protease-degradable peptide, flanked by two cysteine residues (VPM peptide, GCRDVPMSMRGGDRCG, purity 96.9%, Mw 1696.96 Da, GenScript). Cells and/or soluble molecules, such as GFs, were always mixed with the protein and PEGMAL before addition of the crosslinker. Once the crosslinker was added, samples were incubated for 30 min at 37 °C to allow gelation. PEG-only hydrogels were produced as well without the addition of the PEGylated FN. The nomenclature used in this manuscript is: x% (FN) PEG yVPM, x being the percentage of PEGMAL used and y the fraction of degradable crosslinker added. When not indicated, hydrogels were 5% FNPEG 0.5VPM.

2.3. Fibronectin immunostaining

Hydrogels (3, 5 and 10 wt% FNPEG 0VPM or PEG 0VPM only as a control) were embedded in optimal cutting temperature compound (O.C.T compound, VWR) and flash frozen by immersion in liquid nitrogen to preserve the structure of the gel. Samples were stored at −80 °C until use. A cryostat (Leica, −20 °C) was used to cut the samples, and sections 100 μm in thickness were prepared on treated microscope slides (Superfrost™ Plus, ThermoFisher).

FN was detected via immunofluorescence in hydrogel cryosections. Sections were blocked with blocking buffer (1% Bovine Serum Albumin, BSA, Sigma) for 30 min at RT. Then, primary antibody rabbit polyclonal-anti-FN (Sigma, 1:400) was added and incubated for 1 h at RT. Samples were washed three times using washing buffer (0.5% Tween 20 (Sigma) in PBS). Then, secondary antibody goat-anti-rabbit-Cy3 (Jackson ImmunoResearch, 1:200) was incubated for 1 h at RT and protected from light. Samples were washed three times using washing buffer and were mounted with VECTASHIELD mounting media without DAPI (Vector Laboratories). Images were taken with a ZEISS AxioObserver Z.1 at different magnifications.

2.4. Fibronectin release

FN release at 24 h was measured as a way to demonstrate that PEGylated FN was covalently crosslinked to the PEG network. If FN is covalently crosslinked there should not be any FN release, whereas if we add native FN into the hydrogel system, as it is not crosslinked, by diffusion FN should be released. To do so, hydrogels (either 5% FNPEG 0VPM, 5% PEG 0VPM or 5% PEG 0VPM hydrogels with native FN entrapped (PEG + FN)) were immersed for 24 h in PBS to assess the release of FN. Native FN was mixed in solution with the PEGMAL polymer prior to the addition of the crosslinker in order to entrap FN within the PEG hydrogels (PEG + FN condition). Solutions from supernatants were collected and quantified using bicinchoninic acid colorimetric assay (MicroBCA assay kit, ThermoFisher Scientific), following the manufacturer's instructions. Briefly, BSA and FN standards together with samples were loaded onto a 96-well microplate and were mixed with the working reagent. Then, the microplate was sealed and incubated for 2 h at 37 °C. After incubation, the microplate was let to cool down for 20 min at RT, protected from light. The absorbance at 562 nm was measured using a plate reader (BIOTEK). Conditions were prepared in triplicate and samples were measured in triplicate.

2.5. Water absorption

Hydrogels were formed, weighed (m_0) and immersed in milliQ water for up to a week using filtered tubes (Corning® Costar® Spin-X® centrifuge tube filters, cellulose acetate membrane, pore size 0.45 μm). After 24 h, samples were centrifuged at 6500 rpm for 5 min to remove the supernatant from the basket so that only the hydrogel sample remained in the basket holder. Then, sample and basket were weighed, and the mass of the empty basket was subtracted. The amount of water absorbed was calculated as follows:

$$Water\ Sorption\ (\%) = \frac{m_t - m_0}{m_0} * 100 \quad (1)$$

Where m_t is the weight of the hydrogel at a certain time and m_0 the weight of the hydrogel after formation.

2.6. Mechanical properties

Nanoindentation was assessed using atomic force microscopy in force spectroscopy mode (AFM/FS, Nanowizard-3, JPK). Cantilevers (Arrow-TL1-50, spring constant ~ 0.03 N/m, Nano World innovative technologies) were functionalised manually with silicon oxide microbeads (20 mg mL^{-1}, 20 μm diameter, monodisperse, Corpuscular Inc.). The actual stiffness of the cantilever was estimated using the thermal calibration method. Samples tested were 100 μm cryosections fully swollen in milliQ water. Cryosections were thawed for 5 min at RT. A hydrophobic marker (PAP pen, Vectorlabs) was used to surround the sample and milliQ water was added for 15 min. After swelling, samples were rinsed twice with milliQ water to wash off the remaining O.C.T of the cryosection. Measurements were carried out in immersion. Indentation of at least 500 nm were assessed using constant force. The area of the sample was mapped defining squared areas (2500 μm^2, 25 measurements). Five maps per replicate were measured and at least three replicates per sample were tested, unless otherwise noted. The analysis (JPK-SPM processing software) was performed using the Hertz model for a spherical indenter to fit the curves obtained.

2.7. Degradation assays

Hydrogels were formed and swollen overnight in PBS. All samples were weighed before starting the degradation. Then, samples were covered with protease solution (collagenase type I, Gibco, 50 U mL^{-1} in PBS, 37 °C). At each timepoint, all supernatant was removed by centrifugation at 6500 rpm for 5 min and samples were weighed. To continue the experiment, fresh protease solution was added. The degradation rate was calculated as follows:

$$M_{loss}\ (\%) = \frac{M_i - M_t}{M_i} * 100 \quad (2)$$

Where M_{loss} is the percentage of mass lost during degradation, M_i the mass after swelling in milliQ water (initial mass), and M_t, the mass at the different timepoints after the addition of the protease solution.

2.8. Growth factor labelling

In order to study GF binding and release, VEGF or BMP2 (carrier free, R&D Systems) were fluorescently labelled with an amino reactive dye (DyLight® NHS Ester, Thermo Fisher Scientific) following the manufacturer's instructions. Briefly, GFs were dialysed (Mini-A-Lyzer, COMW 10 kDa, ThermoFisher) against 0.05 M Sodium borate buffer at pH 8.5 for 2 h at RT. Then, the appropriate amount of dye was added (as calculated by the manufacturer's guidelines) to the GF solution. The dye and the GF were let to react for 1 h at RT, protected from light. Then, the non-reacted dye was removed by dialysis against PBS for 3 h. The labelled VEGF was aliquoted and stored at −20 °C until use. Fluorescently labelled VEGF or BMP2 were named VEGF-488 or BMP2-488, respectively, in the main text.

2.9. Growth factor release

Hydrogels were prepared, as described in hydrogel formation section above, that incorporate VEGF-488 or BMP2-488. The final concentration of labelled GF loaded was 10 μg mL^{-1} (unless otherwise noticed). Then, samples were immersed in PBS and incubated at 37 °C protected from light. At each timepoint, all the PBS solution was taken and used to measure the fluorescence (Ex/Em 493/518 nm) using a plate reader (BIOTEK). Fresh PBS was added after each timepoint. A standard curve using VEGF-488 or BMP2-488 was prepared and measured together with the samples. An empty condition (not loaded with GF) was used as control. All conditions were prepared in triplicate, and each sample was measured three times. The cumulative release (%) was calculated as follows:

$$GF_{released}(\%) = 100 m_{GFs}/m_{GFi} \quad (3)$$

Where $GF_{released}$ is the percentage of VEGF-488 or BMP2-488 released from hydrogels, m_{GFs} is the amount of VEGF-488 or BMP2-488 measured in the supernatant and m_{GFi} is the amount of VEGF-488 or BMP2-488 initially loaded.

2.10. VEGF uptake

Hydrogels were immersed in 10 mM L-cysteine solution for 2 h to ensure that all the maleimide groups from the hydrogels were reacted. After that, samples were washed three times in PBS and immersed in VEGF-488 solutions of different concentrations (5, 10 and 15 μg mL^{-1}). Once immersed, samples were incubated for 20 h at 37 °C while protected from light. The supernatant was then taken and read using a plate reader (Ex/Em 493/518 nm). All conditions were prepared in quadruplicate and all samples were measured twice. The initial solutions were also measured and used as standard curve to be able to correlate fluorescence intensity with VEGF-488 concentration. The fluorescence intensity of hydrogels immersed in PBS (without VEGF-488) was measured to normalise the data. The percentage of VEGF-488 absorbed was calculated as follows:

$$m_{VEGF\ absorbed} = m_{VEGFi} - m_{VEGFs} \quad (4)$$

Where $m_{VEGF\ absorbed}$ is the final mass of VEGF-488 retained in the hydrogels, m_{VEGFi} is the initial total mass of VEGF-488 added to the samples in solution, and m_{VEGFs} is the total mass of VEGF-488 measured in the supernatant after incubation. Once the amount of VEGF-488 retained in the samples was calculated, the percentage of VEGF-488 absorbed was calculated as follows:

$$VEGF_{absorbed}\ (\%) = 100 - VEGF_{soluble}\ (\%) \quad (5)$$

Where $VEGF_{absorbed}$ is the percentage of VEGF retained in the hydrogel and $VEGF_{soluble}$ is the percentage of VEGF measured from the supernatants after the incubation of VEGF with the hydrogel.

2.11. Cell culture

Human umbilical vein endothelial cells (HUVECs) (Caltag Medsystems, passage 1–5) were used for viability and angiogenesis/vascularisation in vitro assays. HUVECs were grown in growth media (large vessel endothelial cell (LVEC) medium, Caltag Medsystems). Human dermal fibroblasts (HDFs) (Caltag Medsystems, passage 1–6) were used for angiogenesis studies. Both cell types were grown in Dulbecco's modified Eagle's medium (DMEM, Gibco) high glucose without pyruvate and 10% fetal bovine serum (FBS, Gibco) until seeding. Once seeded, LVEC media was used. All media used were supplemented with 1% penicillin/streptomycin (Gibco).

2.12. Cell viability

Cytocompatibility of hydrogels was tested using the Live/Dead assay (ThermoFisher), according to the manufacturer's instructions. Briefly, HUVECs cells were encapsulated at 10^6 cells·mL^{-1} to allow single-cell analysis and were incubated within the hydrogels at different timepoints. For each timepoint, cells were stained with 2 μM Calcein-AM and NucBlue and incubated for 15 min. Samples were washed twice before imaging with a confocal microscope (ZEISS CLSM 880) at 10× magnification. Images were quantified using ImageJ 1.51v (National Institutes of Health, US).

$$Viability\ (\%) = \left({}^{live\ cells}/_{N_{total}} \right) * 100 \quad (6)$$

Being N_{total} the total number of cells in that field of view (alive + dead cells).

2.13. Angiogenesis assays

Angiogenic sprouting was assessed using bead microcarriers [64]. Briefly, HUVECs were mixed with dextran-coated Cytodex 3 microcarriers (Sigma) at a final concentration of 400 cells per bead in 1 mL of growth medium. Cells and beads were mixed gently every 20 min for 4 h at 37 °C. Then, cell-coated beads were transferred to a flask with growth medium and incubated overnight (37 °C and 5% CO2). Before encapsulation, cell-coated beads were washed three times with growth medium. Finally, cell-coated beads were loaded into hydrogels at a final concentration of 400 beads·mL^{-1}. Once the hydrogels were prepared, twenty thousand human dermal fibroblasts were seeded on top following protocol described by others [64,65]. When human dermal fibroblasts were not added to the experiment, sprouting was not observed regardless of the presence of VEGF. Conversely, when only fibroblast are added to the hydrogels (but no VEGF) sprouting does not happen either.

Growth media supplemented with different concentrations of VEGF (0, 50, 500 ng mL^{-1}, R&D Systems) was changed every other day. The assay was monitored every day for four days via brightfield microscopy. Samples were fixed using 4% para-formaldehyde for 30 min at RT and stained for actin (AlexaFluor-488 Phalloidin dilution 1:300) and for the nucleus (NucBlue, LifeTechnologies) for 1 h. Samples were washed three times with 0.5% Tween 20 in PBS and mounted onto glass bottom petri dishes using VECTASHIELD mounting medium (VectorLabs). Samples were imaged using a ZEISS Axio Observer Z1 and were prepared in triplicate. Actin images were used for quantification. They were converted into 8-bit greyscale images using ImageJ. After that, the "Find connected regions" plugin of ImageJ was used with the following parameters: find all regions, do not allow diagonal connections, count only regions with intensity values over 50 (to reduce noise), count only regions with a minimum of 100 connected pixels.

2.14. Vascularisation assays

For vascularisation studies, HUVECs were encapsulated ($5{\cdot}10^6$ cells·mL^{-1}) *in situ* within hydrogels loaded with 200 pmol mL^{-1} VEGF-165 (R&D Systems) or within non-loaded hydrogels (without GF). Samples at days one, two and three were fixed with 4% para-formaldehyde for 30 min at RT and stained for actin and the nucleus. Samples were imaged using confocal microscopy (ZEISS LSM 880) at 10× magnification. Stacks obtained from confocal imaging were analysed using ImageJ 1.51v. Briefly, actin cytoskeleton stacks were opened and segmented using the trainable Weka segmentation 3D plugin. Once the stacks were converted to 8-bit segmented stacks, the segmented objects were quantified using the "3D objects counter" tool with the following parameters: volume (V, μm3), number of voxels/object, surface (S, μm2), number of voxels/surface and centroids. Prior to the quantification, a size exclusion filter was applied, so objects smaller than 500 voxels were not counted (to avoid quantification of segmented background noise). The sphericity (Ψ) of the objects was calculated as follows:

$$\Psi = \frac{\pi^{\frac{1}{3}}(6V)^{2/3}}{S} \quad (7)$$

2.15. Chick chorioallantoic membrane assay

Fertilised chick eggs were received at day seven post-fertilisation (E7). Eggs were kept in an incubator (37.5 °C, 50–60% relative humidity). To perform the chorioallantoic membrane (CAM) assay, eggs were candled to detect and mark the air sac of the chick embryo, and the egg shell was then cut on top of the air sac to expose the CAM. Once the membrane was exposed, each sample was laid carefully on top of the membrane. Samples tested were: 5% PEG 0.5VPM, 5%PEG 0.5VPM with 2.5 μg mL^{-1} VEGF165, 5% FNPEG 0.5VPM, 5% FNPEG 0.5VPM with 2.5 μg mL^{-1} VEGF165 and an empty condition, where the CAMs were exposed but no material was placed on top. After that, the exposed area of the egg with the sample was sealed and labelled. All eggs were incubated for four days (E12), when the membranes were imaged using a stereomicroscope (Leica MZ APO) using X8 and X16 magnification. Six replicates per condition were used; two pictures per replicate at

each magnification used were taken. For the quantification, images at X16 magnification were used and the images were anonymised. The green channel of the RGB picture was chosen for the segmentation as it was the one with the best contrast to detect the capillaries. Segmentation was assessed manually, tracing a black line on top of each capillary. The result of the segmentation was used to quantify the number of branches, the number of junctions, and the number of triple points per image via the skeletonize tool on ImageJ.

2.16. Murine non-healing bone defect model

This experiment was conducted under the Animals (Scientific Procedures) ACT 1986 (ASPel project license n° 70/8638). All murine experiments were conducted under the Animals (Scientific Procedures) ACT 1986 (ASPel project license n° 70/8638) and all the research performed, complied with ethical regulations approved by the University of Glasgow's ethical committee.

2.16.1. Implant preparation

Polyimide implant tubes with lateral holes were used as sleeves to be filled with the hydrogel samples (final volume used 3 μL). The implant tubes were immersed in ethanol and sonicated for 10 min. After sonication, implant tubes were rinsed twice with ethanol and then autoclaved. FN hydrogels (5 wt%, FNPEG 0.5VPM) were loaded with BMP2 (R&D Systems) at a final concentration of 0, 5 or 75 μg mL^{-1} (FNPEG-, FNPEG + or FNPEG + +, respectively). The implants were prepared the day before surgery under sterile laminar flow hood and were kept in PBS and 37 °C, 5% CO_2 until use.

2.16.2. Bone radial segmental defect surgery

C57BL/6 male mice (8 weeks old, Charles River, n = 5 mice/condition) were anaesthetised using isoflurane gas. Under anaesthesia, mice were provided with a dose of buprenorphine and carprofen for pain relief. An incision on the skin was carried out along the forearm and the radius was exposed using a periosteal elevator. The centre of the radius was revealed in order to introduce a 2.5 mm wound in the bone, using a custom-made parallel double-bladed bone cutter. The ulna was left intact. The implant was then placed into the introduced bone defect, abutting its proximal and distal ends. Finally, the wound was closed with a degradable suture. Mice were monitored during the experiment for signs of distress, movement, and weight loss.

2.16.3. Analysis of bone growth

Eight weeks after surgery, bone samples were explanted and fixed in 4% para-formaldehyde and immersed in 70% ethanol. Bone samples were analysed using microcomputer tomography (μCT, Bruker Skyscan Micro X-ray CT), and then decalcified using Krajian solution (citric acid, formic acid) for 3 d, until soft and pliable. They were then paraffin embedded for sectioning. Quantification of the bone volume was performed using the CTAn software (Bruker). In order to ensure that only new bone formation was measured, the volume of interest (VOI) was selected to evaluate a central 2.0 mm length of the 2.5 mm total defect size. For histological analysis, sections (of 7 μm thickness) were stained for haematoxylin-Safranin O-Fast Green. Briefly, sections were deparaffinised and rehydrated in water. Then, Mayer's haematoxylin staining was performed for 8 min and Scott's solution was used for 1 min to blue up the nuclear staining. After that, samples were rinsed in 1% acid alcohol and water. Then, 0.5% fast green solution for 30 s was used to stain collagen and sections were rinsed in 1% acetic acid for 3 s. Finally, 0.1% safranin O solution was used for 5 min to counterstain the cartilage and sections were washed in 70%, 95% and absolute ethanol for 1 min each. Sections were cleared twice with Histo-Clear for 5 min and mounted with DPX mounting media. Sections were then imaged with an EVOS FL microscope (ThermoFisher) at 20× magnification. Whole mounts were stitched together using the Image Composite Editor software.

2.17. Statistical analysis

The statistical analysis was performed using GraphPad Prism 6.01 software. All in vitro experiments were carried out in triplicate unless otherwise noticed. All graphs represent mean ± standard deviation (SD) unless otherwise noted. The goodness of fit of all datasets was assessed via D'Agostino-Pearson Normality test. When comparing three or more groups: normal distributed populations were analysed via analysis of variance test (ANOVA test) performing a Tukey's post hoc test to correct for multiple comparisons; when populations were not normally distributed, a Kruskal-Wallis test was used with a Dunn's post hoc test to correct for multiple comparisons. When comparing only two groups, parametric (normal distributed population, *t*-test) or non-parametric (Mann-Whitney test) tests were performed. Differences among groups are stated as follows: for p-values < 0.05 (*), when p-values < 0.01 (**), for p-values < 0.005 (***), for p-values < 0.001 (****), when differences between groups are not statistically significant (n.s).

3. Results

3.1. Fabrication and characterisation of full-length FN hydrogels

FN was covalently incorporated into a poly(ethylene) glycol (PEG) network via Michael-type addition reaction, where a 4-arm-PEG-maleimide spontaneously reacts with a thiolated crosslinker at physiological pH (Fig. 1a and b, Fig. S1). Maleimide groups were chosen to fabricate the hydrogels because they have higher affinity towards thiol groups and confer shorter gelation times at physiological pH relative to hydrogels fabricated using acrylate groups as demonstrated by Phelps and colleagues [66]. Moreover, Michael-type addition has been previously used to form biologically active and cytocompatible hydrogels [67,68].

Prior to hydrogel formation, the disulfide bonds that hold the FN dimers together were reduced to obtain two FN monomers. FN monomers were then PEGylated via a Michael-type addition reaction by functionalisation of the FN cysteine residues with a molar ratio FN monomer to 4-arm-PEG-maleimide of 1–4 (Fig. S2). This ratio was chosen after preliminary optimisation and to use the minimum amount possible of PEG molecules for PEGylation. As PEGylation is a stochastic process we decided to use Michael-type addition to selectively target cysteine residues on FN. We tested the biological activity of the PEGylated FN (Fig. S3). We used enzyme-linked immunosorbent assay (ELISA) with three monoclonal antibodies targeting different domains of FN (Figs. S3a and b) and found it had similar availability of the cell adhesion-binding site and the GF-binding domain (Figs. S3c and d) to native FN. As expected, differences between native and PEGylated FN were found mainly at the collagen binding site, which was less available in the PEGylated version (Fig. S3e) relative to the native form. This is due to PEG molecules principally binding to the FN type I and II repetitions, which are the domains that contain cysteine residues (Fig. 1a). We did not observe differences between the native and PEGylated FN forms when assessing adhesion and focal adhesion formation in C2C12 cells, demonstrating that cells can fully interact with the protein after PEGylation (Fig. S3f-m). These findings agree with previous work reporting that PEGylated FN retains biological activity in terms of cell adhesion and FN fibril assembly, together with some proteolytic stability [69,70]. It is also noteworthy that full-length proteins are reported to retain high biological activity after the PEGylation process when incorporated into hydrogel systems [63,71,72].

We then assessed the homogeneous distribution of FN within the hydrogel network via immunostaining (Fig. 1c). Hydrogels without FN did not show any staining (Fig. S4a). We also tested the efficiency of binding between FN and PEG by studying the release of FN from the hydrogels after 24 h (Fig. 1d) and the presence of FN in the supernatant after release via electrophoresis and Coomassie blue staining (Fig. S4b).

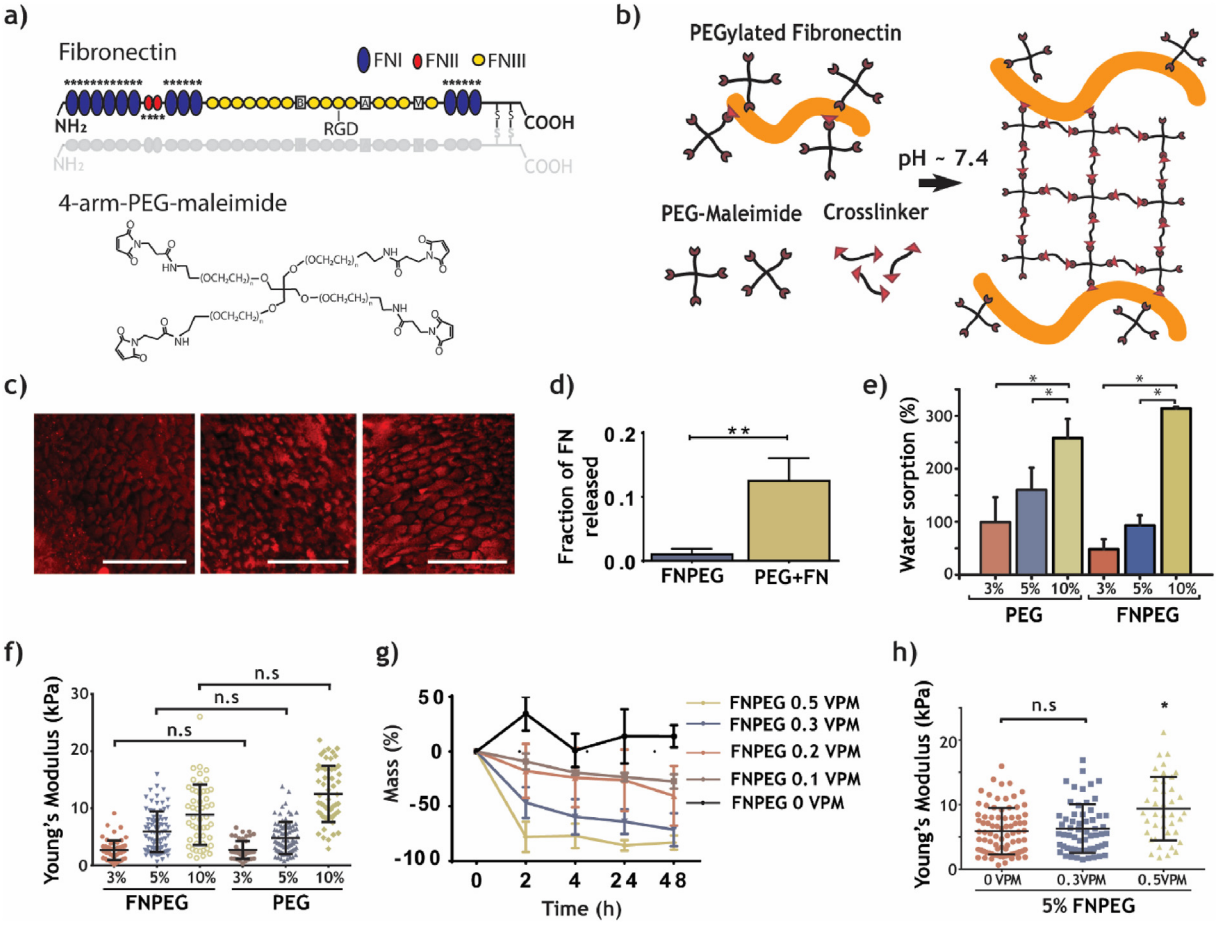

Fig. 1. FN hydrogel formation and characterisation. **(a)** Schematic of the modular composition of FN (upper structure, domains I, II and III are depicted in blue, red and yellow, respectively, and cysteine residues are marked as *), and structure of the 4-arm-PEG-maleimide. **(b)** A schematic of the hydrogel formation protocol, where FN is depicted in orange. **(c)** Immunofluorescence of FN (in red) in cryosections of 3, 5 and 10 wt % FNPEG 0VPM hydrogels (from left to right, scale bar: 100 μm). **(d)** Fraction of FN released after 24 h (mean ± SD, n = 3) from hydrogels into which PEGylated FN had incorporated (FNPEG 0VPM, covalently bound FN) or FN had encapsulated (PEG + FN, non-covalently bound FN, PEG 0VPM hydrogels). **(e)** Water absorption at 24 h of 3, 5 and 10 wt% PEG 0VPM only and FNPEG 0VPM hydrogels (mean ± SD, n = 4). **(f)** Elastic modulus measured by AFM nanoindentation of 3, 5 and 10 wt% PEG only and FNPEG 0VPM hydrogels (mean ± SD, n > 100 curves). **(g)** Degradation profile of FNPEG with different ratios of degradable crosslinker (0, 0.1, 0.2, 0.3, 0.5VPM) (mean ± SD, n = 3). **(h)** FNPEG hydrogels with different ratios of degradable crosslinker (0, 0.3, 0.5VPM) (mean ± SD, n > 100 curves, *p-value < 0.05, ANOVA test followed by a Tukey's post hoc test). FN was covalently incorporated into PEG hydrogels, which could be further tuned to control their stiffness and degradability. (For interpretation of the references to color in this figure legend, the reader is referred to the Web version of this article.)

Hydrogels into which PEGylated FN had incorporated (i.e., covalently bound FN) did not release FN (FNPEG 0VPM, Fig. 1d, Fig. S4b), whereas PEG hydrogels into which native FN was encapsulated (i.e., simply trapped, non-covalently bound FN) released approximately 10% of the initial FN added after 24 h (PEG + FN condition, Fig. 1d).

Using PEG as a hydrogel network allows the physicochemical properties of the system to be controlled [73–75]. Increasing the amount of PEG in the system (from 3 to 10 wt%) increases water absorption in the hydrogels (Fig. 1e), increases Young's modulus (Fig. 1f), both independently of FN, the concentration of which was kept constant in the hydrogels at 1 mg mL^{-1}. As the Young's modulus increases, the mesh size of the hydrogel decreases (Fig. S5). The average Young's modulus (± SD) observed for 3% FNPEG 0VPM hydrogels was 2.6 ± 1.7 kPa and for 3% PEG 0VPM 2.6 ± 1.5 kPa. For 5 wt % hydrogels, the mean Young's modulus obtained was 5.9 ± 3.5 kPa for 5% FNPEG 0VPM and 4.8 ± 2.7 kPa for 5% PEG 0VPM hydrogels. Hydrogels of 10 wt % showed an average Young's modulus of 8.8 ± 5.3 kPa for 10% FNPEG 0VPM hydrogels and 12.5 ± 4.9 kPa for 10% PEG 0VPM hydrogels. These results agree with previously published results on standard PEG hydrogels, where an increase in the PEG percentage resulted in an increase in the Young's modulus [63,73,74,76]. PEG hydrogels can also be engineered to be cell-degradable [12]. To demonstrate controlled levels of degradation, we incorporated a protease degradable crosslinker (VPM peptide, Fig. S1) in combination with thiolated PEG. The degradation rate of hydrogels upon collagenase type I treatment increased with increasing amounts of VPM crosslinker, both for FN-containing hydrogels, FNPEG, and PEG hydrogels without FN (Fig. 1g and Fig. S4d). The addition of increasing ratios of the VPM peptide did not affect either the water sorption ability of the hydrogels (Fig. S4c) nor their mechanical properties up to ratio 0.3VPM (Fig. 1h). We note that ratio 0.5VPM increased the mechanical properties of the hydrogel, from 5.9 ± 3.5 kPa of 0VPM and 6.2 ± 3.7 kPa of 0.3VPM to 9.3 ± 4.9 kPa of 0.5VPM (mean ± SD).

Together, these data demonstrate that full-length and functional FN can be incorporated into a synthetic hydrogel system that has controlled stiffness and degradation rates.

3.2. Full-length FN hydrogels sequester growth factors

As discussed, FN can promiscuously bind GFs, such as VEGF, through the heparin II-binding domain ($FNIII_{12\text{-}14}$) as long as this domain is available for interaction [15,38,40]. We demonstrate the ability

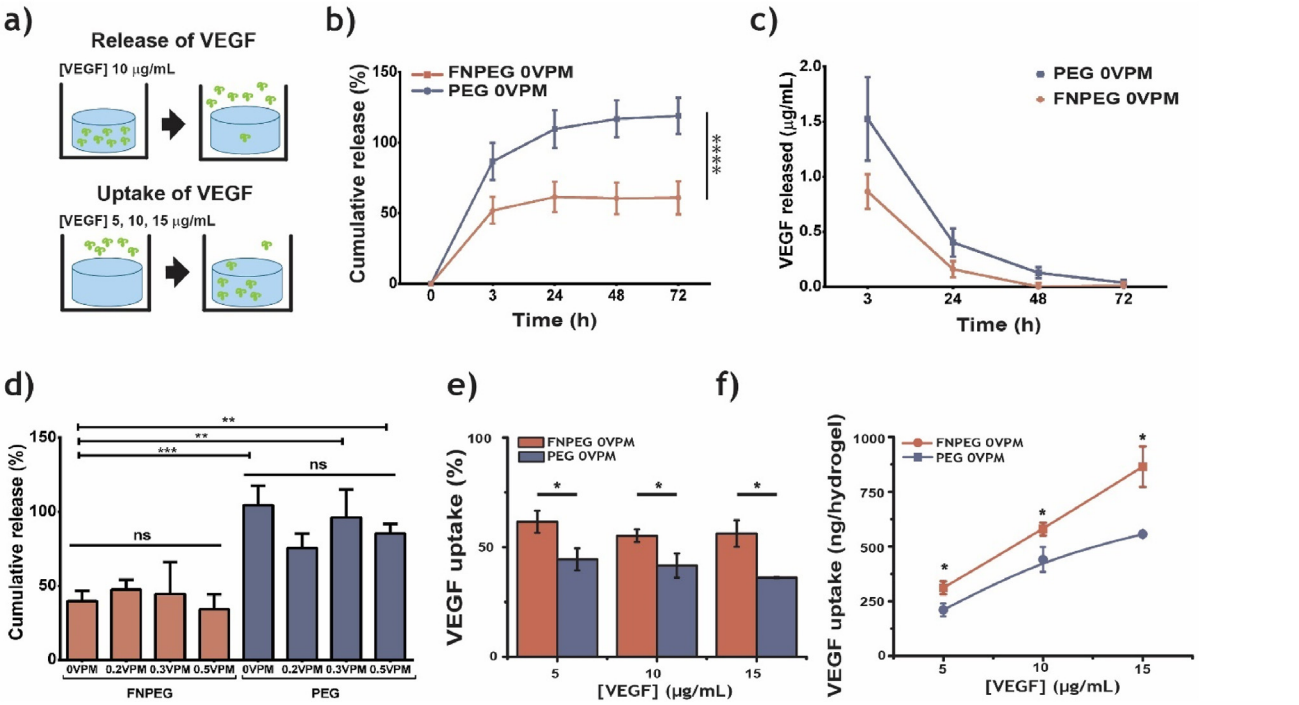

Fig. 2. FN hydrogels actively bind VEGF. **(a)** Schematic of the release experiment in which the hydrogel is loaded with 10 μg/mL of fluorescently labelled VEGF. The hydrogel was then immersed in PBS and the fluorescent intensity of the supernatant tracked through time. Also, schematic of the VEGF uptake assay, in which a hydrogel was immersed in solutions of 5, 10 and 15 μg/mL of fluorescently labelled VEGF and the fluorescence intensity of the supernatant measured. **(b)** The cumulative release of fluorescently labelled VEGF from PEG 0VPM only and FNPEG 0VPM hydrogels, loaded with 10 μg mL^{-1} VEGF (mean ± SD, n = 6, ***p-value < 0.001, Kruskal-Wallis and Dunn's post hoc test). **(c)** Concentrations measured of fluorescently labelled VEGF released from PEG 0VPM only and FNPEG 0VPM (mean ± SD, n = 6). **(d)** Cumulative release of fluorescently labelled VEGF at 64 h from PEG and FNPEG with different ratios of VPM (0, 0.2, 0.3 and 0.5VPM) (mean ± SD, n = 3 ***p-value < 0.001, ANOVA with a Tukey's post hoc test). **(e)** Percentage of VEGF absorbed (*p-value < 0.05, Kruskal-Wallis with a Dunn's post hoc test) and **(f)** amount of VEGF absorbed by PEG 0VPM only and FNPEG 0VPM hydrogels (*p-value < 0.05, Kruskal-Wallis and Dunn's post hoc test). FNPEG hydrogels incorporate VEGF that is stably bound to FN in the 3D environment.

of FN hydrogels to actively sequester GFs, compared to PEG only hydrogels (Fig. 2). VEGF was fluorescently labelled to track its release over time (Fig. 2a). This strategy allowed us to track diffusion of VEGF up to approximately 0.1 μg/mL, according to our standard curve. FNPEG hydrogels retain up to 50% of the VEGF that was initially loaded into the hydrogel, compared to the total release of VEGF from PEG only hydrogels after 24 h (Fig. 2b and c). The release of VEGF probably continues at a slower rate because the isoform used ($VEGF_{165}$) has intermediate affinity to the ECM [77]. We note a burst release during the first 3 h, which is expected in hydrogels. We also note that the presence of VPM peptide did not affect VEGF's sequestration (Fig. 2d), as expected, because we did not use proteases in the experiment. This demonstrates that FNPEG hydrogels can be engineered to control GF presentation independently of their degradability.

We also investigated the release of VEGF from Matrigel and PEG-RGD hydrogels (Fig. S6). PEG-RGD hydrogels were prepared using PEG-MAL and an equivalent amount of RGD peptide to the amount of FN used for FNPEG hydrogels. PEG only and PEG-RGD showed similar release at 72 h, where approximately 75–80% of the VEGF initially loaded was released. On the contrary, Matrigel showed sequestration of VEGF, as it only released 65% of the VEGF loaded. Still, FNPEG hydrogels were able to sequester more VEGF compared to Matrigel and thus, also compared to PEG only and PEG-RGD.

The capability of FNPEG hydrogels to sequester VEGF was further demonstrated in an uptake assay (Fig. 2a). In this assay, hydrogels were immersed in solutions that contained fluorescently labelled VEGF and their absorption was then measured (Fig. 2e and f). FN hydrogels absorbed more VEGF compared to PEG only hydrogels for all concentrations of the initial VEGF solution used (Fig. 2e and f). The increased uptake of VEGF in the FNPEG hydrogels cannot be explained by simple passive diffusion of the GF through the PEG network alone, since both PEG and FNPEG hydrogels absorbed similar amounts of water (Fig. 1e). This demonstrates, together with results from VEGF release experiments, that FN binds VEGF as it diffuses from the initial solution, and that VEGF becomes part of the 'solid phase' of the hydrogel, and allows more GF to diffuse until equilibrium is reached. The difference in VEGF uptake between FNPEG and PEG, as shown in Fig. 2f, for each concentration must be from the VEGF that is bound to FN in the hydrogel. These data show the solid-phase presentation of GFs from crosslinked FN in a synthetic 3D hydrogel with controlled stiffness and degradation rate. To further put in context the differences observed in Fig. 2f, FNPEG hydrogels uptake on average 2 μg of VEGF per mL of hydrogel more than PEG only gels.

In the subsequent experiments, we used only 5 wt% FNPEG and PEG gels with a ratio of 0.5 VPM.

3.3. Full-length FN hydrogels promote microvasculature growth

We next assessed whether having VEGF in FN hydrogels promote endothelial cell activation and microvasculature growth. Human umbilical vein endothelial cells (HUVECs) were encapsulated, *in situ*, in both PEG only and FNPEG hydrogels, and retained high cell viability (Fig. 3a), as expected, due to the mild crosslinking chemistry used to form the hydrogels [78,79]. To investigate endothelial sprouting in 3D, we seeded HUVECs onto microcarrier beads [64,65]. These microcarrier beads are collagen-coated dextran beads hence, HUVECs can attach to the external coating. These cell-coated beads sustain a semi-confluent layer of cells, that were afterwards encapsulated within FNPEG hydrogels or in Matrigel (positive control, Fig. 3b). For this experiment VEGF was supplemented in the media. Qualitatively,

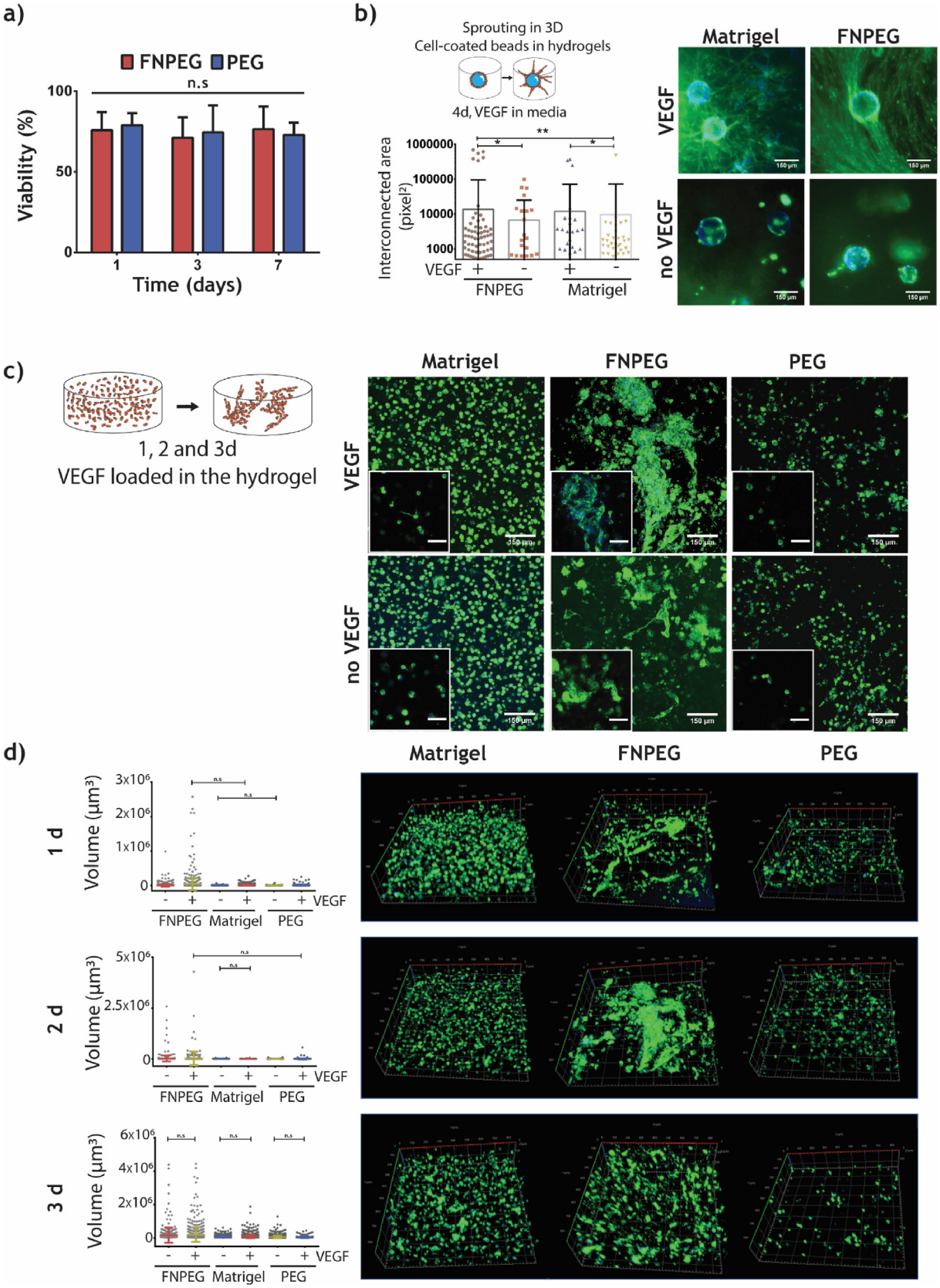

(caption on next page)

Fig. 3. FN hydrogels promote sprouting and microvasculature growth in 3D. **(a)** Percentage viability of HUVECs after encapsulation in FNPEG 0.5VPM and PEG 0.5VPM only hydrogels. **(b)** (Top left) Schematic of 3D sprouting assay, in which HUVECs were seeded onto collagen-coated dextran beads and the cell-coated beads encapsulated in FNPEG 0.5VPM or Matrigel hydrogels. (Right) Representative images of actin cytoskeleton (green) and nucleus (blue) of endothelial cell sprouting within FNPEG 0.5VPM and Matrigel hydrogels with 500 ng/mL VEGF supplemented in the media or no VEGF supplementation (scale bar: 150 μm). (Bottom left) Quantification of sprouting by measuring the connected areas (mean ± SD, *p-value < 0.05, **p-value < 0.01, ANOVA test with Tukey's post hoc test). **(c)** (Left) Schematic of endothelial cell 3D reorganisation assay, in which HUVECs were encapsulated within VEGF-loaded or no-VEGF FNPEG 0.5VPM, Matrigel and PEG 0.5VPM only hydrogels. (Right) Representative z-axis projections of stacks at day 2 post-encapsulation (insets: representative slices of stack images at the same magnification, actin cytoskeleton (green and nucleus (blue)), scale bar: 150 μm. **(d)** (left) Volume of objects (μm^3) at days 1, 2 and 3 after encapsulation, as quantified from stack images, and (right) representative 3D reconstructions of HUVECs within Matrigel, FNPEG 0.5VPM or PEG 0.5VPM at days 1, 2 and 3 (with VEGF) (mean ± SD, n > 100 objects). FN hydrogels are cytocompatible and promote endothelial cell sprouting in 3D at levels comparable to Matrigel. (For interpretation of the references to color in this figure legend, the reader is referred to the Web version of this article.)

FNPEG hydrogels showed high levels of sprouting, similar to those observed in Matrigel (Fig. 3b). Quantitatively, the area covered by connected sprouts was measured using the actin staining. Results from this quantification showed that both FNPEG and Matrigel supplemented with VEGF in the media presented, on average, larger interconnected areas of sprouts. A higher number of very large areas were quantified for the FNPEG condition and Matrigel (supplemented with VEGF), which corresponds to images covered by sprouts as can be seen from the images in Fig. 3b. Comparing FNPEG to Matrigel (both with VEGF) there are more highly connected areas (> 100,000 $pixel^2$), although this was not statistically significant. We note that for both FNPEG hydrogels and Matrigel sprouting only occurred in the presence of 500 ng mL^{-1} VEGF. The use of 50 ng mL^{-1} VEGF resulted in no sprouting in either FNPEG or Matrigel conditions. Comparing our results with others [64,65] and although the amount of VEGF needed in this case was higher (500 ng/mL compared to 1–30 ng/mL [64]), our system provides a well-defined material (for example compared to fibrin clots [64,65]) that requires solely of VEGF in the media to promote sprouting (compared to the addition of VEGF, basic fibroblast GF, angiopoietin-1and transforming growth factor-β used by others [64]).

Next, we investigated whether FNPEG gels promote HUVEC reorganisation in a 3D context, as happens in Matrigel (Fig. 3c and d). To do so, we encapsulated HUVECs and VEGF within FNPEG hydrogels, as well as within Matrigel and PEG controls, and tracked cell morphology at early timepoints. In this case VEGF was loaded directly into the hydrogels together with HUVECs. We found that endothelial cells underwent more extensive morphological and structural changes within the VEGF-containing FNPEG hydrogels, as compared to the cells in the VEGF-containing Matrigel and PEG only hydrogel (Fig. 3c, d and Fig. S7). At days 1 and 2 after encapsulation, endothelial cells within the VEGF-containing FNPEG hydrogels formed multicellular and interconnected structures, as demonstrated in the 3D reconstruction images and volume quantification (Fig. 3d). Endothelial cells did not form these complexes in PEG only (with or without VEGF), although cells in VEGF-containing Matrigel did show some multicellular structures, consisting of 3–4 cells at days 2 and 3. At day 3, the endothelial cell clusters formed in VEGF-containing FNPEG hydrogels started to disassemble, suggesting that these cellular complexes were not stable. During vasculogenesis, endothelial cells are highly dynamic and come together to form primitive capillary structures [80]. However, they require guidance from other cell types, such as pericytes and smooth muscle cells, to stabilise the newly formed capillary [81,82]. These experiments demonstrate that FNPEG hydrogels sequester VEGF and induce endothelial cells to form the early structures associated with vascularisation, more extensively than in cells cultured in Matrigel, even though Matrigel is able to sequester approximately 35% of initial VEGF loaded as shown by release studies (Fig. S6). This suggests that PEG-RGD loaded with VEGF would perform as FNPEG without VEGF, due to its quick release of > 70% of initial VEGF loaded.

After showing that FNPEG hydrogels promote endothelial cell sprouting in 3D, we tested the system in a more complex environment using the chick chorioallantoic membrane (CAM) assay (Fig. 4). Hydrogels (FNPEG hydrogel and PEG control) loaded with VEGF (and controls without VEGF) were placed on top of the exposed CAM, and chick embryos were incubated for four days. For this experiment, where we wanted to assess whether or not the sequestration of VEGF improved capillary formation, PEG hydrogels were used as controls and Matrigel was not included in the experiment.

After incubation, images of the CAM underneath and near the hydrogel were taken and quantified. We note that in some cases hydrogels seemed to have fused with the actual CAM. The results show that increased capillary formation occurred when FNPEG (with or without VEGF) was present, as can be seen by the number of branches and junctions counted per field (Fig. 4c and d). CAMs incubated with VEGF-containing PEG only lacked extensive capillary formation, as seen in the empty condition (when a CAM was exposed but no material was placed on top). This is likely to be due to a rapid release of VEGF from PEG during the first hours, causing VEGF to be lost from the local environment relatively quickly. This would be in accordance with our VEGF release studies (Fig. 2b–d), which showed that VEGF is rapidly released from PEG only hydrogels during the first 24 h. In contrast, FNPEG hydrogels (with or without VEGF) showed the highest levels of capillary formation. This is likely to be due to FNPEG hydrogels providing a more sustainable release of VEGF (as shown in our release studies, Fig. 2b and c) but also because of the likely sequestration of natural VEGF present in the developing CAM [83–85], as also demonstrated in our in vitro VEGF uptake tests (Fig. 2e and f).

3.4. BMP2-loaded FN hydrogels promote bone formation

We used a non-healing (critical size), radial bone defect model in the adult mouse to demonstrate that FNPEG hydrogels promote bone formation in vivo when loaded with low concentrations of BMP2 (Fig. 5). In this model, a 2.5 mm defect was introduced into the radial bone that does not heal spontaneously (Fig. 5d). The ulna was left intact to provide mechanical stabilisation and to avoid the use of additional external fixation plates. Hydrogel-filled implant tubes, 4 mm in length and that contain multiple pores along their sides (Fig. 5b) [39,40,86] were placed inside the bone defect.

To use this model, we first studied the release of BMP2 from the hydrogel system in vitro (Fig. 5a and b). We observed that, for an initial amount of BMP2 of 10 μg/mL, FNPEG hydrogels released approximately 70% of the BMP2 initially loaded into them in the first 4 h, whereas PEG only hydrogels (that do not contain FN) released more than 90% of the BMP2 loaded into them in the same time period (Fig. 5a). We hypothesised that 30% of BMP2 in FNPEG hydrogels remained bound to FN.

We used two initial concentrations of BMP2 for this experiment: 5 and 75 μg/mL (denoted as FNPEG+ and FNPEG++, respectively). Implant tubes were filled with FNPEG hydrogels loaded with BMP2 the day before the experiment (hydrogels without BMP2 were used as a control, denoted FNPEG-). We tracked the release of BMP2 from FNPEG hydrogels at 24 h using the two selected initial concentrations of BMP2, to estimate the amount of BMP2 that remained in the hydrogel prior to implantation (Fig. 5b). FNPEG hydrogels loaded with 5 μg/mL released 27 ± 11% of BMP2 after 24 h and, FNPEG hydrogels loaded with 75 μg/mL released 88 ± 6% of the initial BMP2 after 24 h (mean ± SD). Because some of the BMP2 loaded is released during the first hours

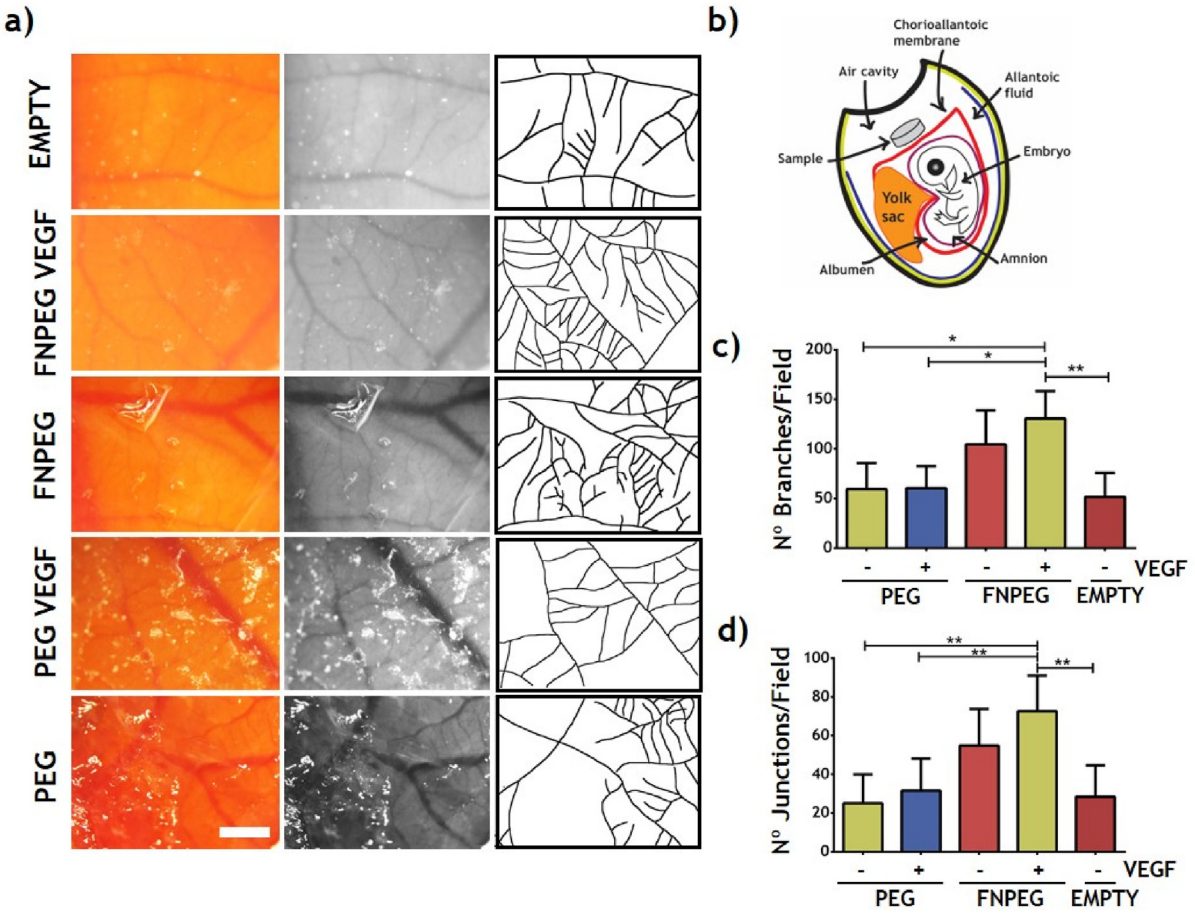

Fig. 4. FN hydrogels promote capillary formation in vivo. (a) Representative images of chick chorioallantoic membrane (CAMs) (left column), green microscopy channel used for quantification (middle column), and (right column) manually drawn images of capillary branching. Conditions tested from top to bottom: "empty" (no hydrogel), "FNPEG VEGF" (FNPEG 0.5 VPM loaded with 125 ng VEGF), "FNPEG" (FNPEG 0.5 VPM), "PEG VEGF" (PEG only 0.5 VPM loaded with 125 ng VEGF) and "PEG" (PEG only 0.5 VPM) (scale bar: 1 mm). (b) Schematic of the chick CAM assay, in which the egg shell is opened to expose the CAM and hydrogel samples are carefully placed on top. (c) Number of branches per image (mean ± SD, n > 10 images) and (d) number of junctions per image (mean ± SD, n > 10 images). FN hydrogels promote capillary formation in the chick chorioallantoic membrane assay.

and because this amount is different depending on the initial amount of BMP2 loaded, we estimated that the FNPEG hydrogels contained 10.5 and 49.5 ng of BMP2 for initial loading of 5 and 75 μg/mL, respectively. This means that the initial concentration of BMP2 in the hydrogels at the time of implantation was 3.5 and 16.5 μg/mL, respectively. We note that 10.5 and 49.5 ng of BMP2 in this bone model can be considered to be ultralow and low doses [39,40].

An analysis of the bone defects implanted with FNPEG++ hydrogels, by micro computed tomography (μCT) scans, showed that the defect was bridged in 2 out of 5 mice tested. When bone defects were implanted with the FNPEG + hydrogels, varying results were recorded, and no closure of the bone gap was observed (Fig. 5e–h). Likewise, the bone gap remained unclosed in the FNPEG- control (Fig. 5e–h). Quantification of bone volume (BV, mm^3) showed that the highest increase in bone formation occurred in the FNPEG++ implanted hydrogels, relative to the FNPEG- (no BMP2) controls (Fig. 5e). Some FNPEG++-implanted bones also showed fusion to the ulna (Fig. 5f). This could be due to the hydrogel swelling and coming into contact with the ulna through the pores of the implant tube. Fusion to the ulna for FNPEG++ in most cases resulted in bone forming also at the outer part of the implant tube. Some bone growth was also observed coming from the ulna in the FNPEG + condition. Although no bone-defect closure was observed in the FNPEG + group, we observed a trend of increased bone growth from FNPEG-, to FNPEG+ and to FNPEG++ that corresponded with increasing amounts of BMP2 in the implants (Fig. 5e).

Longitudinal sections of the paraffin embedded forearms were stained with safranin-O (that stains for cartilage, in red), fast green (that stains for collagen) and haematoxylin (to counterstain the nuclei) (Fig. 5g and h). Fig. 5g shows a whole mount of the implant tube position and greater collagen deposition (stained in blue) in the FNPEG+ and to FNPEG++ implanted bones, relative to the FNPEG- control, which did not stain for collagen around the defect. Fig. 5h shows the formation of new tissue within the implant tube in more detail. Cell infiltration (as denoted by black arrows in Fig. 5h) was observed in the FNPEG- hydrogels along the defect. The structures seen in this condition appear to resemble fat tissue. Some bone matrix deposits were observed at the outer part of the implant, probably to mechanically support the area. This is supported by the presence of osteoclasts at the proximal end of the defect (Fig. S8), which would increase bone resorption in that area (Fig. 5g).

In the FNPEG + condition, compact bone formation was observed along the wall of the implant tube, with osteoblasts present at the outer layer and bone resorption was also observed, as indicated by the presence of osteoclasts (Fig. 5h). This indicates that bone remodelling occurred within the implant tube. Bone marrow cavities were also present, which could indicate normal bone structure formation (Fig. 5h).

In the FNPEG++ condition, implant tubes were filled with compact bone, as well as with new bone and trabecular bone, which filled the gap (Fig. 5g and h). The presence of newly formed bone, together with that of bone marrow cavity structures, demonstrates that normal

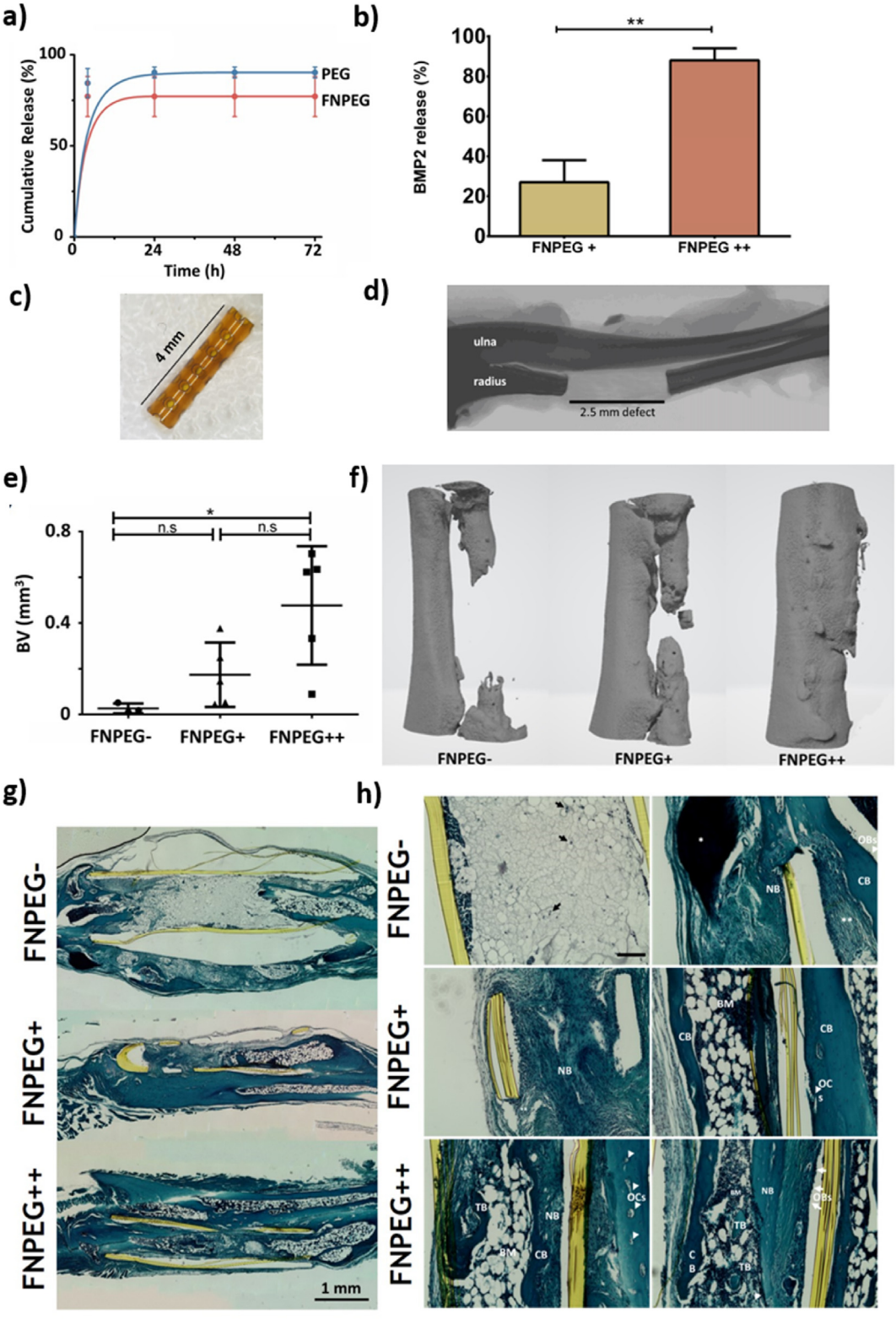

(caption on next page)

bone growth occurred within the implant tube. An endosteum-like structure was observed next to the implant tube wall, which was surrounded by osteoblasts, osteoclasts and compact bone. These results suggest that low doses of BMP2 within these matrices can support normal bone growth.

4. Discussion

We have developed a platform to engineer hydrogels that incorporate full-length FN within a synthetic polymer network and that display controlled physico-chemical properties. FN has been extensively used as a coating of surfaces and hydrogels in 2D mechanotransduction studies [18,19]. The field is in need of biomaterials that replace

Fig. 5. FN hydrogels promote bone growth in vivo. **(a)** Cumulative release of fluorescently labelled BMP2 from FNPEG 0VPM hydrogels and PEG 0VPM only hydrogels (%, mean ± SD, n = 4). **(b)** Percentage release of fluorescently labelled BMP2 at 24 h when loading 5 and 75 μg/mL of BMP2 in FNPEG 0.5VPM hydrogels. **(c)** Picture of an implant tube to be filled with hydrogels. **(d)** Scheme of the critical-size defect model, where the radius is segmentally cut creating a 2.5 mm defect but leaving the ulna intact. **(e)** The percentage of bone volume (BV) quantified in FNPEG- (no BMP2, control FNPEG 0.5VPM), and in FNPEG + and FNPEG + + hydrogels (FNPEG 0.5VPM), which were initially loaded with 10.5 and 49.5 ng of BMP2, respectively (mean ± SD, n = 5, *p-value 0.0086). **(f)** 3D reconstructions of micro computed tomography (μCT) scans showing 4 mm of the ulna (left) and the radius (right), where the implant tube was placed. **(g)** Whole mount, longitudinal sections of representative forearms, with the proximal end to the left (scale bar: 1 mm). Yellow colour shows the walls of the implant tube. **(h)** Representative histological images of bone repair in each treatment group and the FNPEG- control (showing safranin O, fast green and haematoxylin staining) (scale bar: 100 μm). Black arrows show cell infiltration, * indicates bone deposition, ** marks fibrotic tissue, NB shows new bone formation, CB shows compact bone, OBs are osteoblasts indicated by white arrows, OCs are osteoclasts indicated by white arrowheads, TB shows trabecular bone, and BM shows bone marrow cavities. These results show that FN hydrogels promote bone growth at low BMP2 concentrations. (For interpretation of the references to color in this figure legend, the reader is referred to the Web version of this article.)

Matrigel and can be used to engineer reproducible 3D environments that support cellular complex processes, such as regeneration, development and cancer studies. Fibrinogen is critically used in vivo as its use is approved by the FDA for some applications (e.g. tissue sealant) as opposed to Matrigel that is mostly used for in vitro applications. In this regard, fibrinogen has been incorporated into a synthetic PEG hydrogel that further improved classic fibrin gels as the biophysical properties were fully defined because of the use of PEG as a backbone in which fibrinogen was incorporated [41,75]. PEG-based hydrogels functionalised with simple adhesive peptides (e.g. RGD) have also shown to support complex biological structures such as intestinal organoids [87,88]. Alternatively, a hyaluronic acid-based hydrogel has been developed as a platform for in vitro breast cancer culture [89]. These systems have been successful in developing Matrigel alternatives. However, using just PEG functionalised with adhesive peptides might not recapitulate the full properties of the ECM and the HA-based hydrogels show limitations in controlling mechanical properties. Both of them have limited affinity for growth factors, an essential aspect in the successful performance of Matrigel. These limitations are overcome by the use of FN-based hydrogels developed here.

To covalently incorporate FN into a PEG network, PEGylation of FN has been reported in literature targeting either lysine residues [90] or cysteine residues [91], resulting in biologically active FN. FN is denatured during our PEGylation procedure (Fig. S2a). However, FN has the capability of refolding after denaturation. Patel et al. characterised the differences between native FN and refolded fibronectin (i.e. FN after a denaturing-renaturing cycle) [92,93]. They found no differences in the content of secondary structure, the affinity for gelatin or the capability of FN to form fibrils. They also found evidence of higher affinity of refolded FN for heparin. These findings suggest that FN's structure can change during denaturation/PEGylation steps but still be able to maintain several biological activities. The selection of cysteine residues as target amino acid for the PEGylation step confers good selectivity as cysteine residues are well characterised within the FN molecule. By using thiol-PEGylation we are targeting specific regions on fibronectin as all FNI and FNII domains contain two disulphide bonds, whereas FNIII domains do not contain any [48]. This means the cell binding and GF binding regions are not affected by PEGylation (Fig. S3).

FN was previously grafted into a hyaluronic acid hydrogel for 3D cell culture [72]. To do this, they also PEGylated FN. They targeted primary amines, which makes PEGylation unspecific, and added a 10-fold molar excess of PEG for PEGylation. However, there was not enough characterisation about the biological activities of FN after PEGylation (e.g. availability of the integrin and GF binding domain). Critically, the FN hydrogels reported here allow the use of FN in controlled 3D environments and so can be used as controlled ECM mimetic to extend mechanotransduction studies to 3D environments and develop in vitro tissue models avoiding the use of uncontrolled matrices such as Matrigel. These hydrogels are synthetic and tuneable, as shown by the characterisation of its mechanical properties and degradation profiles (Fig. 1 and Fig. S4). We demonstrate that full-length FN can be covalently linked to these hydrogels without altering their key biological activities. Our ELISAs (Figs. S3a–e) confirm that PEGylation occurred mainly at the FNI and FNII domains (e.g. when using MAB1892 there is a difference in antibody affinity comparing native and PEGylated FN, while antibodies HFN7.1 and P5F3 that target FNIII domains show similar affinity between native and PEGylated fibronectin). From our cell adhesion studies (Fig. S3f-m) C2C12 cells are able to adhere and form focal adhesions when seeded on top of PEGylated FN.

FN is a homodimer that presents a globular conformation in solution (e.g. in plasma). FN in globular conformation contains some important domains hidden such as the $FNIII_{12\text{-}14}$ (i.e. the GF binding domain). However, FN needs to change its conformation in order to expose those cryptic domains that are unavailable in the globular conformation. Therefore, FN fibrillogenesis, a cell-mediated process were FN is polymerised in 3D by cells, is essential to make these domains available [94].

We demonstrate the efficacy of the system in two demanding applications, in 3D culture in vitro and in bone regeneration in vivo. We show that FN hydrogels sequester VEGF from the environment and promote vascularisation efficiently, both in vitro and in vivo. From our release assays, we have observed differences in the capability of FNPEG hydrogels to sequester VEGF and BMP2 (Fig. 2, Fig. S6 and Fig. 5a and b). It has been previously shown that BMP2 has higher affinity to FN compared to VEGF, which is contrary to what our release studies suggest as VEGF is retained more in the hydrogels [15]. This could be explained because of the different molecular weight (BMP2 has lower molecular weight than VEGF). This could factor in a quicker release of BMP2 since there is a burst release during the first hours. This is in accordance with our data obtained from release experiments of BMP2 with different concentrations of BMP2 (Fig. 5a and b). Additionally, another VEGF binding site on FN has been identified [95]. Mitsi et al. found two types of VEGF-FN binding, one constitutively available and another controlled by changes in conformation of FN. They also showed that hydrophilic substrates increased a more extended conformation of FN, which they found to enhance VEGF binding. This could explain the differences seen in our release experiments for VEGF and BMP2. PEGylated VEGF was used as a strategy to deliver VEGF upon protease cleavage in PEG-based hydrogels [82]. In this case VEGF delivered from PEG-RGD performed poorly compared to VEGF-free GFOGER-PEG hydrogels for vascularisation in a bone defect in vivo. Taking into account the poor performance of PEG-RGD in literature studying similar hydrogels (4- arm-PEG-maleimide using Michael-type addition reaction) [82] and our data showing a quick release of VEGF from PEG-RGD hydrogels (Fig. S6), we did not include PEG-RGD in our studies.

FN hydrogels loaded with low concentrations of BMP2 can also promote bone growth in a non-healing mouse bone defect model. Note here that Matrigel was not selected as a control condition due to its lack of potential translatability. Few studies use Matrigel with bone morphogenetic proteins, for example Langenfeld et al. used Matrigel together with BMP2 to assess the promotion of angiogenesis in tumours [96]. In this regard, fibrinogen-based hydrogels [63], which was one of the first attempts to engineer protein-based synthetic hydrogels seeking to recapitulate features of the ECM, have been used to load BMP2 for bone regeneration. This was used to achieve regenerative effect in an athymic nude mice (immunodeficient) cranial defect model [41].

However, FN offers synergy between integrin and GF receptors [25,40] which allows ultralow doses of GFs to be used (e.g. we used 10.5 ng and 49.5 ng of BMP2 per implant to achieve regenerative effects in a murine (wild type) non-healing radial defect model). To contextualise the amounts of BMP2 used in our in vivo study, Shekaran and colleagues used similar hydrogels (4-arm-PEG-maleimide based hydrogels) loaded with BMP2 and used the same murine radial bone defect model [86]. They first compared the performance for osteogenesis in vitro of these PEG hydrogels combined with either the GFOGER peptide or RGD peptide (even at 2 mM concentration) and they observed that GFOGER-PEG hydrogels promoted greater osteogenesis than PEG-RGD. For the critical size defect model they loaded 20, 40 and 200 μg/mL of BMP2 into the GFOGER-PEG hydrogels, considering 20 μg/mL low dose of BMP2.

Similarly, Cheng et al. used a murine femoral critical size defect model to study the delivery of BMP2 and testosterone in bone regeneration [97]. They used a polypropylene fumarate (PPF)/tricalcium phosphate (TCP) scaffold to load either BMP2, BMP2 and testosterone or testosterone alone. In this case, they reported that the best condition had both BMP2 and testosterone (5 and 10 μg, respectively). Another example of co-delivery of BMP2 was reported by Zwingenberger et al., where they used a murine femoral critical size defect model [98]. Here, they considered 2.5 μg a low dose of BMP2, which was loaded into a heparinized mineralized collagen type I matrix. They observed greater bone formation when co-delivering BMP2 and stroma cell-derived factor-1 (SDF-1α) (2.5 and 10 μg, respectively). Ben-David et al., used PEG-fibrinogen loaded with low dose of BMP-2 in a critical size calvarial defect model (5 mm diameter defect, 1.5 mm thick, 1 μg of BMP2, 8 μg/mL) [41].

It remains for future studies to address whether bone regeneration could be improved by further optimising the initial amount of BMP2 loaded into the implant tube, and whether the generation of stiffer hydrogels could promote osteogenesis by the stem cells available at the fracture site. We note that the presence of FN in our hydrogels provide cell attachment, as it would happen in a PEG-RGD hydrogel. However, in growth factor release experiments comparing PEG, PEG-RGD and FNPEG (Fig. S6), we obtained that PEG-RGD had a similar release to PEG only, which suggests that the amount of GF in the hydrogel would be too low to play a significant biological role. This hypothesis is in line with results published on PEG-RGD hydrogels, where they found poor osteogenesis from PEG-RGD hydrogels that led the authors to investigate PEG-GFOGER hydrogels instead [86].

5. Conclusion

Overall, our findings demonstrate that GFs can be efficiently presented in a highly controllable, fully synthetic, 3D microenvironment for use in multiple tissue-engineering applications. The FN hydrogel system has the potential to substitute Matrigel in 3D culture models, given that it is a chemically defined system that contains full-length proteins and distinct, solid-phase, presentation of GFs. This system can also be produced using purified human recombinant proteins, removing the need to screen for pathogens as occurs when using Matrigel matrices. The chemistries used to form the hydrogels are mild, cytocompatible and spontaneous at physiological pH and temperature. Moreover, the FN-based hydrogels are transparent, and so are well-suited for colorimetric/fluorometric assays. Being a biosynthetic system, it has the potential to be more amenable for translation in e.g. drug testing platforms or tissue engineering [87].

Data availability

All the original data related to this article are within the depository of the University of Glasgow https://doi.org/10.5525/gla.researchdata.906.

CRediT authorship contribution statement

Sara Trujillo: Conceptualization, Methodology, Investigation, Writing - original draft. **Cristina Gonzalez-Garcia:** Methodology, Investigation. **Patricia Rico:** Methodology, Investigation. **Andrew Reid:** Investigation. **James Windmill:** Methodology, Supervision. **Matthew J. Dalby:** Conceptualization, Methodology, Writing - original draft, Supervision. **Manuel Salmeron-Sanchez:** Conceptualization, Methodology, Writing - original draft, Supervision, Funding acquisition.

Declaration of competing interest

The authors declare that they have no known competing financial interests or personal relationships that could have appeared to influence the work reported in this paper.

Acknowledgements

This study was supported by the UK Regenerative Medicine Platform (MRC grant MR/L022710/1), the UK Engineering and Physical Sciences Research Council (EPSRC EP/P001114/1) and a programme grant from the Sir Bobby Charlton Foundation. μCT work was supported by the European Research Council (ERC) under the European Union's Seventh Framework Programme (FP7/2007-2013) (grant agreement No. [615030]). S.T. acknowledges support from the University of Glasgow through their internal scholarship funding program. We thank the support of David Adams (Anatomy lab, University of Glasgow) and the Biological Services and Veterinary Research Facility (University of Glasagow) for their assistance.

Appendix A. Supplementary data

Supplementary data to this article can be found online at https://doi.org/10.1016/j.biomaterials.2020.120104.

References

[1] B. Weigelt, C.M. Ghajar, M.J. Bissell, The need for complex 3D culture models to unravel novel pathways and identify accurate biomarkers in breast cancer, Adv. Drug Deliv. Rev. (2014) 69–70, https://doi.org/10.1016/j.addr.2014.01.001 42–51.

[2] M. Jarad, E.A. Kuczynski, J. Morrison, A.M. Viloria-Petit, B.L. Coomber, Release of endothelial cell associated VEGFR2 during TGF-β modulated angiogenesis in vitro, BMC Cell Biol. 18 (2017) 1–10, https://doi.org/10.1186/s12860-017-0127-y.

[3] J.R. Spence, C.N. Mayhew, S.A. Rankin, M.F. Kuhar, J.E. Vallance, K. Tolle, E.E. Hoskins, V.V. Kalinichenko, S.I. Wells, A.M. Zorn, N.F. Shroyer, J.M. Wells, Directed differentiation of human pluripotent stem cells into intestinal tissue in vitro, Nature 470 (2011) 105–110, https://doi.org/10.1038/nature09691.

[4] S.J. Yang, J.K. Son, S.J. Hong, N.E. Lee, D.Y. Shin, S.H. Park, S.B. An, Y.C. Sung, J.B. Park, H.M. Yang, S.J. Kim, Ectopic vascularized bone formation by human umbilical cord-derived mesenchymal stromal cells expressing bone morphogenetic factor-2 and endothelial cells, Biochem. Biophys. Res. Commun. 504 (2018) 302–308, https://doi.org/10.1016/j.bbrc.2018.08.179.

[5] C.S. Hughes, L.M. Postovit, G.A. Lajoie, Matrigel: a complex protein mixture required for optimal growth of cell culture, Proteomics 10 (2010) 1886–1890, https://doi.org/10.1002/pmic.200900758.

[6] M.J. Dalby, A.J. García, M. Salmeron-Sanchez, Receptor control in mesenchymal stem cell engineering, Nat. Rev. Mater. 3 (2018), https://doi.org/10.1038/natrevmats.2017.91.

[7] M.M. Martino, S. Brkic, E. Bovo, M. Burger, D.J. Schaefer, T. Wolff, L. Gürke, P.S. Briquez, H.M. Larsson, R. Gianni-Barrera, J.A. Hubbell, A. Banfi, Extracellular matrix and growth factor engineering for controlled angiogenesis in regenerative medicine, Front. Bioeng. Biotechnol. 3 (2015) 1–8, https://doi.org/10.3389/fbioe.2015.00045.

[8] J. Hartikainen, Vascular Endothelial Growth Factors Biology and Current Status of Clinical Applications in Cardiovascular Medicine vol. 49, (2007), https://doi.org/10.1016/j.jacc.2006.09.053.

[9] A.C. Mitchell, P.S. Briquez, J.A. Hubbell, J.R. Cochran, Engineering growth factors for regenerative medicine applications, Acta Biomater. (2016), https://doi.org/10.1016/j.actbio.2015.11.007.

[10] K.H. Sprugel, J.M. McPherson, A.W. Clowes, R. Ross, Effects of growth factors in vivo. I. Cell ingrowth into porous subcutaneous chambers, Am. J. Pathol. (1987).

[11] M.M. Martino, P.S. Briquez, K. Maruyama, J.A. Hubbell, Extracellular matrix-inspired growth factor delivery systems for bone regeneration, Adv. Drug Deliv. Rev.

94 (2015) 41–52, https://doi.org/10.1016/j.addr.2015.04.007.
[12] A.K. Jha, K.M. Tharp, S. Browne, J. Ye, A. Stahl, Y. Yeghiazarians, K.E. Healy, Matrix metalloproteinase-13 mediated degradation of hyaluronic acid-based matrices orchestrates stem cell engraftment through vascular integration, Biomaterials 89 (2016) 136–147, https://doi.org/10.1016/j.biomaterials.2016.02.023.
[13] M.M. Martino, P.S. Briquez, A. Ranga, M.P. Lutolf, J.A. Hubbell, Heparin-binding domain of fibrin(ogen) binds growth factors and promotes tissue repair when incorporated within a synthetic matrix, Proc. Natl. Acad. Sci. 110 (2013) 4563–4568, https://doi.org/10.1073/pnas.1221602110.
[14] L. De Laporte, J.J. Rice, F. Tortelli, J.A. Hubbell, Tenascin C Promiscuously Binds Growth Factors via its Fifth Fibronectin Type III-like Domain, (2013), p. 8, https://doi.org/10.1371/journal.pone.0062076.
[15] M.M. Martino, J.A. Hubbell, The 12th-14th type III repeats of fibronectin function as a highly promiscuous growth factor-binding domain, Faseb. J. 24 (2010) 4711–4721, https://doi.org/10.1096/fj.09-151282.
[16] G. Altankov, F. Grinnell, T. Groth, Studies on the biocompatibility of materials: fibroblast reorganization of substratum-bound fibronectin on surfaces varying in wettability, J. Biomed. Mater. Res. 30 (1996) 385–391, https://doi.org/10.1002/(SICI)1097-4636(199603)30:3<385::AID-JBM13>3.0.CO;2-J.
[17] D.J. Donaldson, J.T. Mahan, Fibrinogen and fibronectin as substrates for epidermal cell migration during wound closure, J. Cell Sci. 62 (1983) 117–127.
[18] A. Elosegui-Artola, R. Oria, Y. Chen, A. Kosmalska, C. Pérez-González, N. Castro, C. Zhu, X. Trepat, P. Roca-Cusachs, Mechanical regulation of a molecular clutch defines force transmission and transduction in response to matrix rigidity, Nat. Cell Biol. 18 (2016) 540–548, https://doi.org/10.1038/ncb3336.
[19] D. Missirlis, J.P. Spatz, Combined effects of PEG hydrogel elasticity and cell-adhesive coating on fibroblast adhesion and persistent migration, Biomacromolecules 15 (2014) 195–205, https://doi.org/10.1021/bm4014827.
[20] L. Baugh, V. Vogel, Structural changes of fibronectin adsorbed to model surfaces probed by fluorescence resonance energy transfer, J. Biomed. Mater. Res. - Part A. 69 (2004) 525–534, https://doi.org/10.1002/jbm.a.30026.
[21] D. Faulón Marruecos, M. Kastantin, D.K. Schwartz, J.L. Kaar, Dense poly(ethylene glycol) brushes reduce adsorption and stabilize the unfolded conformation of fibronectin, Biomacromolecules 17 (2016) 1017–1025, https://doi.org/10.1021/acs.biomac.5b01657.
[22] M. Bieniek, V. Llopis-Hernandez, K. Douglas, M. Salmeron-Sanchez, C. Lorenz, Minor chemistry changes alter surface hydration to control fibronectin adsorption and assembly into nanofibrils, Adv. Theor. Simulat. (2019) 1–13, https://doi.org/10.1002/adts.201900169 1900169.
[23] B.G. Keselowsky, D.M. Collard, A.J. García, Surface chemistry modulates fibronectin conformation and directs integrin binding and specificity to control cell adhesion, J. Biomed. Mater. Res. Part A (2003), https://doi.org/10.1002/jbm.a.10537.
[24] R.N. Wang, J. Green, Z. Wang, J. Ye, Z. Yan, S. Denduluri, O. Idowu, M. Li, C. Shen, A. Hu, R.C. Haydon, R. Kang, J. Mok, M.J. Lee, H.L. Luu, L.L. Shi, Bone Morphogenetic Protein (BMP) signaling in development and human diseases, Genes Dis. 1 (2014) 87–105, https://doi.org/10.1016/j.gendis.2014.07.005.
[25] M.M. Martino, F. Tortelli, M. Mochizuki, S. Traub, D. Ben-David, G.A. Kuhn, R. Müller, E. Livne, S.A. Eming, J.A. Hubbell, Engineering the growth factor microenvironment with fibronectin domains to promote wound and bone tissue healing, Sci. Transl. Med. 3 (2011), https://doi.org/10.1126/scitranslmed.3002614.
[26] E.S. Wijelath, S. Rahman, M. Namekata, J. Murray, T. Nishimura, Z. Mostafavi-Pour, Y. Patel, Y. Suda, M.J. Humphries, M. Sobel, Heparin-II domain of fibronectin is a vascular endothelial growth factor-binding domain: enhancement of VEGF biological activity by a singular growth factor/matrix protein synergism, Circ. Res. 99 (2006) 853–860, https://doi.org/10.1161/01.RES.0000246849.17887.66.
[27] E.S. Wijelath, S. Rahman, J. Murray, Y. Patel, G. Savidge, M. Sobel, Fibronectin promotes VEGF-induced CD34+cell differentiation into endothelial cells, J. Vasc. Surg. (2004), https://doi.org/10.1016/j.jvs.2003.10.042.
[28] E.S. Wijelath, J. Murray, S. Rahman, Y. Patel, A. Ishida, K. Strand, S. Aziz, C. Cardona, W.P. Hammond, G.F. Savidge, S. Rafii, M. Sobel, Novel vascular endothelial growth factor binding domains of fibronectin enhance vascular endothelial growth factor biological activity, Circ. Res. (2002), https://doi.org/10.1161/01.RES.0000026420.22406.79.
[29] A. Stejskalová, N. Oliva, F.J. England, B.D. Almquist, Biologically Inspired , Cell-Selective Release of Aptamer-Trapped Growth Factors by Traction Forces, (2019), p. 1806380, https://doi.org/10.1002/adma.201806380.
[30] T. Crouzier, K. Ren, C. Nicolas, C. Roy, C. Picart, Layer-by-layer films as a biomimetic reservoir for rhBMP-2 delivery: controlled differentiation of myoblasts to osteoblasts, Small 5 (2009) 598–608, https://doi.org/10.1002/smll.200800804.
[31] E.A. Phelps, N. Landazuri, P.M. Thule, W.R. Taylor, A.J. Garcia, Bioartificial matrices for therapeutic vascularization, Proc. Natl. Acad. Sci. 107 (2010) 3323–3328, https://doi.org/10.1073/pnas.0905447107.
[32] G.A. Foster, D.M. Headen, C. González-García, M. Salmerón-Sánchez, H. Shirwan, A.J. García, Protease-degradable microgels for protein delivery for vascularization, Biomaterials 113 (2017) 170–175, https://doi.org/10.1016/j.biomaterials.2016.10.044.
[33] J.R. García, A.J. García, Biomaterial-mediated strategies targeting vascularization for bone repair, Drug Deliv. Transl. Res. 6 (2016) 77–95, https://doi.org/10.1007/s13346-015-0236-0.
[34] M. Salmerón-Sánchez, M.J. Dalby, Synergistic growth factor microenvironments, Chem. Commun. (2016), https://doi.org/10.1039/c6cc06888j.
[35] Y. Mao, J.E. Schwarzbauer, Fibronectin fibrillogenesis, a cell-mediated matrix assembly process, Matrix Biol. (2005), https://doi.org/10.1016/j.matbio.2005.06.008.
[36] P. Singh, C. Carraher, J.E. Schwarzbauer, Assembly of fibronectin extracellular marix, Annu. Rev. Cell Dev. Biol. 26 (2010) 397–419, https://doi.org/10.1146/annurev-cellbio-100109-104020.
[37] V. Llopis-Hernández, M. Cantini, C. González-García, M. Salmerón-Sánchez, Material-based strategies to engineer fibronectin matrices for regenerative medicine, Int. Mater. Rev. 60 (2015) 245–264, https://doi.org/10.1179/1743280414Y.0000000049.
[38] V. Moulisová, C. Gonzalez-García, M. Cantini, A. Rodrigo-Navarro, J. Weaver, M. Costell, R. Sabater i Serra, M.J. Dalby, A.J. García, M. Salmerón-Sánchez, Engineered microenvironments for synergistic VEGF – integrin signalling during vascularization, Biomaterials 126 (2017) 61–74, https://doi.org/10.1016/j.biomaterials.2017.02.024.
[39] Z.A. Cheng, A. Alba-perez, C. Gonzalez-garcia, H. Donnelly, V. Llopis-hernandez, V. Jayawarna, P. Childs, D.W. Shields, M. Cantini, L. Ruiz-cantu, A. Reid, J.F.C. Windmill, E.S. Addison, S. Corr, W.G. Marshall, M.J. Dalby, M. Salmeron-sanchez, Nanoscale Coatings for Ultralow Dose BMP-2-Driven Regeneration of Critical-Sized Bone Defects, (2019), p. 1800361, https://doi.org/10.1002/advs.201800361.
[40] V. Llopis-hernández, M. Cantini, C. González-garcía, Z.A. Cheng, J. Yang, P.M. Tsimbouri, A.J. García, M.J. Dalby, M. Salmerón-sánchez, Material-driven Fibronectin Assembly for High-Efficiency Presentation of Growth Factors vols. 1–10, (2016).
[41] D. Ben-David, S. Srouji, K. Shapira-Schweitzer, O. Kossover, E. Ivanir, G. Kuhn, R. Müller, D. Seliktar, E. Livne, Low dose BMP-2 treatment for bone repair using a PEGylated fibrinogen hydrogel matrix, Biomaterials 34 (2013) 2902–2910, https://doi.org/10.1016/j.biomaterials.2013.01.035.
[42] C.M. Klass, J.R. Couchman, A. Woods, Control of extracellular matrix assembly by syndecan-2 proteoglycan, J. Cell Sci. (2000).
[43] A. Woods, R.L. Longley, S. Tumova, J.R. Couchman, Syndecan-4 binding to the high affinity heparin-binding domain of fibronectin drives focal adhesion formation in fibroblasts, Arch. Biochem. Biophys. (2000), https://doi.org/10.1006/abbi.1999.1607.
[44] J.L. Guan, R.O. Hynes, Lymphoid cells recognize an alternatively spliced segment of fibronectin via the integrin receptor α4β1, Cell (1990), https://doi.org/10.1016/0092-8674(90)90715-Q.
[45] E.A. Wayner, A. Garcia-Pardo, M.J. Humphries, J.A. McDonald, W.G. Carter, Identification and characterization of the T lymphocyte adhesion receptor for an alternative cell attachment domain (CS-1) in plasma fibronectin, J. Cell Biol. (1989), https://doi.org/10.1083/jcb.109.3.1321.
[46] A. Hielscher, K. Ellis, C. Qiu, J. Porterfield, S. Gerecht, Fibronectin deposition participates in extracellular matrix assembly and vascular morphogenesis, PloS One 11 (2016) 1–27, https://doi.org/10.1371/journal.pone.0147600.
[47] X. Zhou, R.G. Rowe, N. Hiraoka, J.P. George, D. Wirtz, D.F. Mosher, I. Virtanen, M.A. Chernousov, S.J. Weiss, Fibronectin fibrillogenesis regulates three-dimensional neovessel formation, Genes Dev. 22 (2008) 1231–1243, https://doi.org/10.1101/gad.1643308.
[48] R. Pankov, Fibronectin at a glance, J. Cell Sci. 115 (2002) 3861–3863, https://doi.org/10.1242/jcs.00059.
[49] M.K. Magnusson, D.F. Mosher, Fibronectin: structure, assembly, and cardiovascular implications, Arterioscler. Thromb. Vasc. Biol. 18 (1998) 1363–1370, https://doi.org/10.1161/01.ATV.18.9.1363.
[50] M. Leiss, K. Beckmann, A. Girós, M. Costell, R. Fässler, The role of integrin binding sites in fibronectin matrix assembly in vivo, Curr. Opin. Cell Biol. 20 (2008) 502–507, https://doi.org/10.1016/j.ceb.2008.06.001.
[51] G.S. Krishnakumar, A. Roffi, Clinical Application of Bone Morphogenetic Proteins for Bone Healing : a Systematic Review, (2017), pp. 1073–1083, https://doi.org/10.1007/s00264-017-3471-9.
[52] K.S. Cahill, J.H. Chi, A. Day, E.B. Claus, Prevalence, complications and hospital charges associated with use of bone-morphogenetic proteins in spinal fusion procedures, J. Am. Med. Assoc. 302 (2009) 58–66.
[53] A.W. James, G. Lachaud, J. Shen, G. Asatrian, V. Nguyen, Z. Xinli, K. Ting, C. Soo, A review of the clinical side effects of bone morphogenetic protein-2, Tissue Eng. Part B Rev. 22 (2016) 284–297, https://doi.org/10.1089/ten.teb.2015.0357.
[54] K.A. Kyburz, K.S. Anseth, Synthetic mimics of the extracellular matrix: how simple is complex enough? Ann. Biomed. Eng. 43 (2015) 489–500, https://doi.org/10.1007/s10439-015-1297-4.
[55] M.J. Dalby, A.J. García, M. Salmeron-Sanchez, Receptor control in mesenchymal stem cell engineering, Nat. Rev. Mater. (2018), https://doi.org/10.1038/natrevmats.2017.91.
[56] H. Shegarfi, O. Reikeras, Review article: bone transplantation and immune response, J. Orthop. Surg. (2016), https://doi.org/10.1177/230949900901700218.
[57] C. Myeroff, M. Archdeacon, Autogenous bone graft: donor sites and techniques, J. Bone Jt. Surg. - Ser. A (2011), https://doi.org/10.2106/JBJS.J.01513.
[58] R. Dimitriou, G.I. Mataliotakis, A.G. Angoules, N.K. Kanakaris, P.V. Giannoudis, Complications following autologous bone graft harvesting from the iliac crest and using the RIA: a systematic review, Injury (2011), https://doi.org/10.1016/j.injury.2011.06.015.
[59] A.S. Curry, N.W. Pensa, A.M. Barlow, S.L. Bellis, Taking cues from the extracellular matrix to design bone-mimetic regenerative scaffolds, Matrix Biol. 52–54 (2016) 397–412, https://doi.org/10.1016/j.matbio.2016.02.011.
[60] S.S. Lee, E.L. Hsu, M. Mendoza, J. Ghodasra, M.S. Nickoli, A. Ashtekar, M. Polavarapu, J. Babu, R.M. Riaz, J.D. Nicolas, D. Nelson, S.Z. Hashmi, S.R. Kaltz, J.S. Earhart, B.R. Merk, J.S. Mckee, S.F. Bairstow, R.N. Shah, W.K. Hsu, S.I. Stupp, Gel scaffolds of BMP-2-binding peptide amphiphile nanofibers for spinal arthrodesis, Adv. Healthc. Mater. (2015), https://doi.org/10.1002/adhm.201400129.
[61] E.S. Sani, P. Lara, E.S. Sani, R.P. Lara, Z. Aldawood, S.H. Bassir, An antimicrobial

dental light curable bioadhesive hydrogel for treatment of Peri- implant diseases an antimicrobial dental light curable bioadhesive hydrogel for treatment of Peri-implant diseases, Matter (2019) 1–19, https://doi.org/10.1016/j.matt.2019.07.019.
[62] L. Wang, H. Fan, Z.Y. Zhang, A.J. Lou, G.X. Pei, S. Jiang, T.W. Mu, J.J. Qin, S.Y. Chen, D. Jin, Osteogenesis and angiogenesis of tissue-engineered bone constructed by prevascularized β-tricalcium phosphate Scaffold and mesenchymal stem cells, Biomaterials (2010), https://doi.org/10.1016/j.biomaterials.2010.08.036.
[63] L. Almany, D. Seliktar, Biosynthetic hydrogel scaffolds made from fibrinogen and polyethylene glycol for 3D cell cultures, Biomaterials 26 (2005) 2467–2477, https://doi.org/10.1016/j.biomaterials.2004.06.047.
[64] M.N. Nakatsu, R.C.A. Sainson, J.N. Aoto, K.L. Taylor, M. Aitkenhead, S. Pérez-del-Pulgar, P.M. Carpenter, C.C.W. Hughes, Angiogenic sprouting and capillary lumen formation modeled by human umbilical vein endothelial cells (HUVEC) in fibrin gels: the role of fibroblasts and Angiopoietin-1, Microvasc. Res. 66 (2003) 102–112, https://doi.org/10.1016/S0026-2862(03)00045-1.
[65] S. Li, L.R. Nih, H. Bachman, P. Fei, Y. Li, E. Nam, R. Dimatteo, S.T. Carmichael, T.H. Barker, T. Segura, Hydrogels with precisely controlled integrin activation dictate vascular patterning and permeability, Nat. Mater. 16 (2017) 953–961, https://doi.org/10.1038/nmat4954.
[66] E.A. Phelps, N.O. Enemchukwu, V.F. Fiore, J.C. Sy, N. Murthy, T.A. Sulchek, T.H. Barker, A.J. García, Maleimide cross-linked bioactive PEG hydrogel exhibits improved reaction kinetics and cross-linking for cell encapsulation and in situ delivery, Adv. Mater. 24 (2012) 64–70, https://doi.org/10.1002/adma.201103574.
[67] L.E. Jansen, L.J. Negrón-Piñeiro, S. Galarza, S.R. Peyton, Control of thiol-maleimide reaction kinetics in PEG hydrogel networks, Acta Biomater. 1133 (2018), https://doi.org/10.1016/j.actbio.2018.01.043.
[68] E.A. Phelps, K.L. Templeman, P.M. Thulé, A.J. García, Engineered VEGF-releasing PEG–MAL hydrogel for pancreatic islet vascularization, Drug Deliv. Transl. Res. 5 (2015) 125–136, https://doi.org/10.1007/s13346-013-0142-2.
[69] C. Zhang, A. Ramanathan, N.W. Karuri, Proteolytically stabilizing fibronectin without compromising cell and gelatin binding activity, Biotechnol. Prog. 31 (2015) 277–288, https://doi.org/10.1002/btpr.2018.
[70] C. Zhang, R. Desai, V. Perez-Luna, N. Karuri, PEGylation of lysine residues improves the proteolytic stability of fibronectin while retaining biological activity, Biotechnol. J. 9 (2014) 1033–1043, https://doi.org/10.1002/biot.201400115.
[71] A.T. Francisco, P.Y. Hwang, C.G. Jeong, L. Jing, J. Chen, L.A. Setton, Photocrosslinkable laminin-functionalized polyethylene glycol hydrogel for intervertebral disc regeneration, Acta Biomater. 10 (2014) 1102–1111, https://doi.org/10.1016/j.actbio.2013.11.013.
[72] S.K. Seidlits, C.T. Drinnan, R.R. Petersen, J.B. Shear, L.J. Suggs, C.E. Schmidt, Fibronectin-hyaluronic acid composite hydrogels for three-dimensional endothelial cell culture, Acta Biomater. 7 (2011) 2401–2409, https://doi.org/10.1016/j.actbio.2011.03.024.
[73] M.P. Lutolf, J.A. Hubbell, Synthesis and physicochemical characterization of end-linked poly(ethylene glycol)-co-peptide hydrogels formed by Michael-type addition, Biomacromolecules 4 (2003) 713–722, https://doi.org/10.1021/bm025744e.
[74] E. Cambria, K. Renggli, C.C. Ahrens, C.D. Cook, C. Kroll, A.T. Krueger, B. Imperiali, L.G. Griffith, Covalent modification of synthetic hydrogels with bioactive proteins via sortase-mediated ligation, Biomacromolecules 16 (2015) 2316–2326, https://doi.org/10.1021/acs.biomac.5b00549.
[75] R. Goldshmid, D. Seliktar, Hydrogel Modulus Affects Proliferation Rate and Pluripotency of Human Mesenchymal Stem Cells Grown in Three-Dimensional Culture, (2017), https://doi.org/10.1021/acsbiomaterials.7b00266.
[76] J.E. Leslie-Barbick, J.J. Moon, J.L. West, Covalently-immobilized vascular endothelial growth factor promotes endothelial cell tubulogenesis in poly(ethylene glycol) diacrylate hydrogels, J. Biomater. Sci. Polym. Ed. 20 (2009) 1763–1779, https://doi.org/10.1163/156856208X386381.
[77] N. Ferrara, H.P. Gerber, J. LeCouter, The biology of VEGF and its receptors, Nat. Med. 9 (2003) 669–676, https://doi.org/10.1038/nm0603-669.
[78] J.E. Leslie-barbick, J.J. Moon, J.L. West, Covalently-Immobilized vascular endothelial growth factor promotes endothelial cell tubulogenesis in poly (ethylene glycol) diacrylate hydrogels, J. Biomater. Sci. Polym. Ed. 20 (2009) 1763–1779, https://doi.org/10.1163/156856208X386381.
[79] E.A. Phelps, A.J. García, Engineering more than a cell: vascularization strategies in tissue engineering, Curr. Opin. Biotechnol. 21 (2010) 704–709, https://doi.org/10.1016/j.copbio.2010.06.005.
[80] N. Ferrara, R.S. Kerbel, Angiogenesis as a therapeutic target, Nature 438 (2005) 967–974, https://doi.org/10.1038/nature04483.
[81] G.L. Semenza, Vasculogenesis, angiogenesis, and arteriogenesis: mechanisms of blood vessel formation and remodeling, J. Cell. Biochem. 102 (2007) 840–847, https://doi.org/10.1002/jcb.21523.
[82] J.R. García, A.Y. Clark, A.J. García, Integrin-specific hydrogels functionalized with VEGF for vascularization and bone regeneration of critical-size bone defects, J. Biomed. Mater. Res. Part A (2016), https://doi.org/10.1002/jbm.a.35626.
[83] D. Ribatti, The chick embryo chorioallantoic membrane (CAM). A multifaceted experimental model, Mech. Dev. 141 (2016) 70–77, https://doi.org/10.1016/j.mod.2016.05.003.
[84] O. Baum, F. Suter, B. Gerber, S.A. Tschanz, R. Buergy, F. Blank, R. Hlushchuk, V. Djonov, VEGF-A Promotes Intussusceptive Angiogenesis in the Developing Chicken Chorioallantoic Membrane, (2010), pp. 447–457, https://doi.org/10.1111/j.1549-8719.2010.00043.x.
[85] C. Marinaccio, B. Nico, D. Ribatti, Differential Expression of Angiogenic and Anti-angiogenic Molecules in the Chick Embryo Chorioallantoic Membrane and Selected Organs during Embryonic Development vol. 916, (2014), pp. 907–916, https://doi.org/10.1387/ijdb.130317dr.
[86] A. Shekaran, J.R. García, A.Y. Clark, T.E. Kavanaugh, A.S. Lin, R.E. Guldberg, A.J. García, Bone regeneration using an alpha 2 beta 1 integrin-specific hydrogel as a BMP-2 delivery vehicle, Biomaterials 35 (2014) 5453–5461, https://doi.org/10.1016/j.biomaterials.2014.03.055.
[87] R. Cruz-Acuña, M. Quirós, A.E. Farkas, P.H. Dedhia, S. Huang, D. Siuda, V. García-Hernández, A.J. Miller, J.R. Spence, A. Nusrat, A.J. García, Synthetic hydrogels for human intestinal organoid generation and colonic wound repair, Nat. Cell Biol. 19 (2017) 1326–1335, https://doi.org/10.1038/ncb3632.
[88] R. Cruz-Acuña, M. Quirós, S. Huang, D. Siuda, J.R. Spence, A. Nusrat, A.J. García, PEG-4MAL hydrogels for human organoid generation, culture, and in vivo delivery, Nat. Protoc. 13 (2018) 2102–2119, https://doi.org/10.1038/s41596-018-0036-3.
[89] A.E.G. Baker, L.C. Bahlmann, R.Y. Tam, J.C. Liu, A.N. Ganesh, N. Mitrousis, R. Marcellus, M. Spears, J.M.S. Bartlett, D.W. Cescon, G.D. Bader, M.S. Shoichet, Benchmarking to the gold standard: hyaluronan-oxime hydrogels recapitulate xenograft models with in vitro breast cancer spheroid culture, Adv. Mater. 1901166 (2019) 1901166, https://doi.org/10.1002/adma.201901166.
[90] C. Zhang, S. Hekmatfar, A. Ramanathan, N.W. Karuri, PEGylated human plasma fibronectin is proteolytically stable, supports cell adhesion, cell migration, focal adhesion assembly, and fibronectin fibrillogenesis, Biotechnol. Prog. (2013), https://doi.org/10.1002/btpr.1689.
[91] C. Zhang, S. Hekmatfer, N.W. Karuri, A comparative study of polyethylene glycol hydrogels derivatized with the RGD peptide and the cell-binding domain of fibronectin, J. Biomed. Mater. Res. - Part A. 102 (2014) 170–179, https://doi.org/10.1002/jbm.a.34687.
[92] S. Patel, A.F. Chaffotte, F. Goubard, E. Pauthe, Urea-Induced sequential unfolding of fibronectin: a fluorescence spectroscopy and circular dichroism study, Biochemistry 43 (2004) 1724–1735, https://doi.org/10.1021/bi0347104.
[93] S. Patel, A.F. Chaffotte, B. Amana, F. Goubard, E. Pauthe, In vitro denaturation-renaturation of fibronectin. Formation of multimers disulfide-linked and shuffling of intramolecular disulfide bonds, Int. J. Biochem. Cell Biol. 38 (2006) 1547–1560, https://doi.org/10.1016/j.biocel.2006.03.005.
[94] J.E. Schwarzbauer, Identification of the fibronectin sequences required for assembly of a fibrillar matrix, J. Cell Biol. (1991), https://doi.org/10.1083/jcb.113.6.1463.
[95] M. Mitsi, Z. Hong, C.E. Costello, M.A. Nugent, Heparin-mediated conformational changes in fibronectin expose vascular endothelial growth factor binding sites, Biochemistry (2006), https://doi.org/10.1021/bi060974p.
[96] E.M. Langenfeld, J. Langenfeld, Bone morphogenetic protein-2 stimulates angiogenesis in developing Tumors11NIH K22 grant CA91919-01A1 and UMDNJ Foundation to J. Langenfeld, Mol. Cancer Res. 2 (2004) 141 LP – 149 http://mcr.aacrjournals.org/content/2/3/141.abstract.
[97] B.H. Cheng, T.M.G. Chu, C. Chang, H.Y. Kang, K.E. Huang, Testosterone delivered with a scaffold is as effective as bone morphologic protein-2 in promoting the repair of critical-size segmental defect of femoral bone in mice, PloS One 8 (2013) 1–10, https://doi.org/10.1371/journal.pone.0070234.
[98] S. Zwingenberger, R. Langanke, C. Vater, G. Lee, E. Niederlohmann, M. Sensenschmidt, A. Jacobi, R. Bernhardt, M. Muders, S. Rammelt, S. Knaack, M. Gelinsky, K.P. Günther, S.B. Goodman, M. Stiehler, The effect of SDF-1α on low dose BMP-2 mediated bone regeneration by release from heparinized mineralized collagen type I matrix scaffolds in a murine critical size bone defect model, J. Biomed. Mater. Res. - Part A. (2016), https://doi.org/10.1002/jbm.a.35744.